Examining the role of autophagy in modulating apoptotic signaling and skeletal muscle recovery after cardiotoxin injury in tamoxifen-inducible, skeletal muscle-specific Atg7 knockdown mice

by

Troy Campbell

A thesis
presented to the University of Waterloo
in fulfillment of the
thesis requirement for the degree of
Master of Science
in
Kinesiology

Waterloo, Ontario, Canada, 2015

Author's declaration

I hereby declare that I am the sole author of this thesis. This is a true copy of the thesis, including any required final revisions, as accepted by my examiners.

I understand that my thesis may be made electronically available to the public.

Troy Campbell

Abstract

Skeletal muscle is a unique tissue composed of multinucleated, post-mitotic fibers. Despite its post-mitotic nature, skeletal muscle has an astounding ability to regenerate after injury largely thanks to muscle-specific stem cells known as satellite cells. Skeletal muscle also constantly balances rates of protein synthesis and breakdown in order to maintain its viability. One of the major systems involved in muscle protein degradation is autophagy. During autophagy, long-lived and damaged cellular components are sequestered in double membrane bound vesicles known as autophagosomes and are subsequently degraded by lysosomes. The E1-like enzyme known as ATG7 (autophagy-related protein 7) is critical to this process as it plays a key role in autophagosome formation. Autophagy has important metabolic functions, but it also plays a major role in cell quality control in order to reduce cell stress and a form of cell death known as apoptosis. Apoptosis can be induced by a number of internal and/or external signals, and leads to the cleavage of a variety of different proteins within the cell. Many points of interaction exist between apoptosis and autophagy which has led to increased examination of the interplay between the two processes. Conclusions from these studies have caused a divergence in opinion regarding the protective or toxic role of autophagy in times of stress in various tissues, including skeletal muscle. Consequently, the aim of the current thesis was to investigate the role of autophagy in modulating apoptotic signaling and skeletal muscle recovery in response to cardiotoxin-induced muscle damage. To do this, tamoxifen-inducible, skeletal muscle-specific Atg7 knockdown mice (i.e. F/F^{Cre} mice) generated using Cre-lox technology were compared to control mice (i.e. F/F mice) prior to and 3, 7, and 14 days after cardiotoxin-induced skeletal muscle injury. This model was shown to be quite effective in knocking down the Atg7 gene, as ATG7 protein was reduced by ~61% in the F/F^{Cre} mice relative to the F/F control mice prior to

cardiotoxin exposure. Unexpectedly, a restoration of ATG7 expression was observed in the F/F^{Cre} mice by day 3 post-injury. It is speculated that this return of ATG7 protein was caused by the recruitment of satellite cells to the muscle fibers in response to damage, as the induction of Atg7 knockdown likely did not occur in these cells. It is also possible that Cre-mediated recombination of Atg7 did not occur in all of the myonuclei, and in turn, $Atg7^{+/+}$ myonuclei could have upregulated ATG7 production after cardiotoxin exposure. Although the restoration of ATG7 in the F/F^{Cre} mice prevented the current study from examining changes in apoptotic signaling and muscle recovery in response to autophagy inhibition, it was still possible to examine the relationship between autophagy and apoptosis in response to acute muscle damage. Autophagic signaling appeared to peak on day 3 post-cardiotoxin injury and then began to decrease over time. In contrast, apoptotic signaling was only slightly elevated on day 3, and did not peak until day 7 when autophagic activity was decreasing. These findings, in combination with reduced cytochrome c, MnSOD, and CuZnSOD on day 3, as well as reduced tBid expression on day 3 and 7, may suggest that autophagy plays a cytoprotective role after muscle damage by suppressing cell stress and apoptotic signaling. Additionally, the results of the current study suggest that basal autophagy inhibition could potentially alter fiber type distribution and cause reductions in muscle mass, while a subsequent restoration of autophagy could return muscle fiber type composition and muscle mass to control levels. Overall, this thesis was able to further elucidate the temporal relationship between autophagic and apoptotic signaling after acute muscle injury, and was able to evaluate the effects of basal autophagy inhibition on muscle mass and muscle fiber type distribution. Valuable methodological information for future studies planning to use inducible, skeletal muscle-specific gene knockout models in conditions of extensive muscle damage can also be drawn from the results of this thesis.

Acknowledgements

First and foremost I would like to thank my family. I know with 100% certainty that I would not be the person I am today without them and their endless support. Mom, Dad, Cory, Linda, Will, Norma, Connor, and everyone else, I cannot thank you enough.

Secondly, I would like to thank my supervisor Dr. Joe Quadrilatero and my committee members Dr. Jim Rush and Dr. Paul Spagnuolo for their time and recommendations which allowed me to complete this thesis. I would also like to thank everyone else who was involved in the completion of my thesis, my amazing lab members, and my great friends who have made the last few years some of the best of my life. Finally, I would like to thank Dr. Jack Callaghan and Dr. Dave Frost for giving me my initial opportunity in research.

Table of Contents

List of figures

Introduction

Skeletal muscle

Skeletal muscle is a highly metabolically active tissue that constitutes 40-50% of total body mass[1]. It is a unique tissue composed of multinucleated, post-mitotic fibers that functions to facilitate movement, breathing, and control of posture[2]. Contraction of skeletal muscle can cause tissue damage that needs to be repaired in order for the muscle to function optimally[3]. Interestingly, despite its post-mitotic nature, skeletal muscle possesses an astounding ability to regenerate itself in response muscle damage[4].

The regeneration of skeletal muscle is facilitated by a specialized population of muscle stem cells known as satellite cells (SCs)[5]. These cells are located between the sarcolemma and the basal lamina of muscle fibers, and remain quiescent under normal conditions[5]. However, satellite cells can become activated and begin to proliferate in response to muscle injury[5]. It is believed that this activation is caused in part by decreased inhibitory signals due to the destruction of the satellite cell niche, and due to the production of activating factors at the basal lamina[5]. Once activated, satellite cells are able to proliferate, differentiate, and fuse with one another to create new myofibers, or fuse to existing fibers to provide them with myonuclei to support regeneration[6]. Furthermore, these cells have the ability to self-renew, as some of the proliferating satellite cells will return to the satellite cell compartment and once again become quiescent[5]. This feature provides skeletal muscle with the ability to deal with degeneration and injury throughout the life cycle[5].

Another important feature of skeletal muscle is its ability to balance rates of protein anabolism and catabolism in order to create a level of protein turnover that maintains the tissue's

viability, mass, and function[7]. Protein synthesis is required to maintain a homeostatic environment as it allows for the production of various cellular components[8], while protein degradation is equally important in order to remove long-lived and damaged proteins and reduce cell stress[8, 9]. In muscle, the two major proteolytic systems are the ubiquitin-proteasome system and autophagy[10].

The ubiquitin-proteasome system and autophagy

The ubiquitin-proteasome system (UPS) degrades proteins through the multi-enzyme complex known as the proteasome[11]. However, in order for this degradation to occur, proteins must first be tagged for destruction via covalent attachment of polyubiquitin chains by E3 ubiquitin ligase enzymes[11]. Although a large number of E3 ligases exist, two that are particularly important in skeletal muscle are muscle atrophy F-box (MAFbx/atrogin-1) and muscle RING finger 1 (MuRF1)[11, 12]. Both of these enzymes have been shown to be increased in conditions of muscle atrophy[13].

Autophagy is a highly regulated, catabolic process that is vital for tissue homeostasis[14]. During this process, an isolation membrane, otherwise known as a "phagophore", elongates within the cytoplasm and sequesters cellular components (e.g. proteins, organelles) before maturing into a double membrane bound vesicle known as an autophagosome[14]. The autophagosome then fuses with a lysosome resulting in the formation of an autophagolysosome. Lysosomal enzymes then degrade the cellular components isolated within the autophagosome[14].

A unique feature of autophagy is that the process contains two ubiquitin-like conjugation systems that facilitate elongation of the phagophore[15]. Autophagy-related (ATG) proteins play a large role in both of these systems. The first system involves the formation of a complex

containing ATG12, ATG5, and ATG16. In this system, the E1-like enzyme ATG7 binds to and activates ATG12, which is then transferred to the E2-like enzyme ATG10 and is finally conjugated with ATG5. The ATG12- ATG5 conjugate then associates with ATG16 to form the ATG12-ATG5-ATG16 complex[15]. In the second system, a protein known as LC3 is first synthesized as pro-LC3 and is then processed by ATG4 into LC3-I, the cytosolic form of the protein. LC3-I is then activated by the E1-like enzyme ATG7, passed on to the E2-like enzyme ATG3, and then is conjugated to phosphatidylethanolamine with the aid of the ATG12-ATG5-ATG16 complex (which acts as an E3-like enzyme of LC3). This results in the formation of the autophagosomal membrane-bound form of LC3 known as LC3-II[15]. Dysfunction in either of these systems can disrupt the autophagic response as they are both essential for autophagosome formation[16]. For example, disruption of the Atg7 gene results in an inhibition of LC3-I conjugation, impaired autophagosome formation, and autophagy suppression[17-21].

One of the fundamental functions of autophagy is to mobilize substrates for ATP production during times of nutrient deficiency (i.e. starvation)[22]. A study by Lum and colleagues helped to solidify this starvation-induced role. This group demonstrated that IL-3 dependent cells that were unable to take in sufficient nutrients due to IL-3 withdrawal were able to maintain their ATP production and viability for a period of time by upregulating autophagy[23]. Although it was originally believed that autophagy only supported ATP production through breakdown of proteins into amino acids, recent research has shown that autophagy is also able to produce metabolic substrates by breaking down carbohydrates and lipids[24]. In addition to providing metabolic substrates, autophagy also helps to maintain cell viability during times of starvation by using mobilized amino acids to synthesize proteins which help the cell adapt to the starvation environment[25].

Along with its metabolic function, autophagy is also involved in cell quality control[26]. Basal autophagy facilitates the degradation of long-lived cytoplasmic contents and damaged organelles and proteins[26]. Accumulation of these damaged cellular products leads to cytotoxic effects, and in turn, the turnover and removal of these products by autophagy helps to decrease stress signaling and prevent cell death processes, including a form of cell death known as apoptosis[27].

Apoptosis

Apoptosis is a highly controlled form of cell death that is important in tissue development and homeostasis[28]. This form of cell death is regulated by a family of cysteine proteases known as caspases, which have been shown to play an essential role in both the initiation and execution of apoptosis[29]. These proteases are involved in a signaling cascade in which a variety of protein substrates are cleaved which leads to the eventual induction of apoptotic cell death[30]. Activation of this signaling cascade can occur in response to both internal and external signals[29]. The main pathway leading to caspase-dependent apoptosis is known as the mitochondrial stress pathway. This pathway is characterized by mitochondrial outer membrane permeabilization (MOMP) as a result of pore formation in the outer mitochondrial membrane[31]. This pore formation is regulated by pro- and anti-apoptotic members of the Bcl-2 family of proteins, which can be subdivided based on the number of Bcl-2 homology (BH) domains that these proteins contain[31]. The anti-apoptotic proteins in this family (e.g. Bcl-2, Bcl-xL) contain all four BH domains (i.e. BH1-BH4), while the pro-apoptotic proteins contain 2-3 BH domains (e.g. the multidomain proteins Bax and Bak) or contain only the BH3 domain (e.g. the BH3-only proteins Bid and Bim)[31]. In response to apoptotic signals, pro-apoptotic Bcl-2 family proteins insert themselves into the outer mitochondrial membrane and form pores[31]. This leads to the release of pro-apoptotic factors like

cytochrome c into the cytosol, resulting in the activation of caspase-9 which then cleaves and activates caspase-3; a critical enzyme in promoting cell death[32]. Anti-apoptotic proteins such as Bcl-2 and Bcl-xL can inhibit this pore formation, cytochrome c release, and subsequent apoptosis by inhibiting the pro-apoptotic proteins at the level of the mitochondria[33]. The endoplasmic reticulum (ER) stress pathway is another internal apoptotic pathway that leads to an accumulation of damaged proteins which causes endoplasmic reticulum stress. This results in the activation of calpains, caspase-12, and eventually caspase-3 causing apoptosis[34]. Finally, in the externally stimulated death receptor pathway, ligands in the extracellular space such as TNF-α and FasL bind to their respective receptors located on the plasma membrane which leads to caspase-8 and caspase-3 activation, and ultimately apoptosis[34].

In addition to caspase-dependent apoptosis, there are also caspase-independent forms of apoptosis initiated at the mitochondria. During caspase-independent apoptosis, pore formation in the mitochondria leads to the release of molecules such as apoptosis-inducing factor (AIF) and endonuclease G (EndoG) into the cytosol[34]. These molecules then translocate to the nucleus and directly cause DNA fragmentation, resulting in apoptotic cell death[34].

Points of interaction between autophagy and apoptosis

Despite different signaling and seemingly different roles, several points of interaction exist between the autophagic and apoptotic pathways[33]. Beclin-1 is a key example of this interplay. Beclin-1 is one of the proteins, along with Vps34, Vps15, and potentially Ambra1, that is incorporated into the Beclin-1 core complex[35]. The formation of this complex is essential for autophagy as it activates the phosphatidylinositide 3-kinase (PI3K) Vps34, which produces phosphatidylinositol-3-phosphate (PI3P)[35]. The production of this phospholipid molecule is

important as it recruits a variety of proteins that facilitate the preliminary steps of autophagosome formation (i.e. upstream of the conjugation systems mentioned above)[15]. As discussed earlier, Bcl-2 and Bcl-xL are both examples of anti-apoptotic proteins, however, these two proteins also possess anti-autophagic properties as they contain BH3-binding grooves which can interact with the BH3 domain of Beclin-1 and inhibit autophagy[33]. In order to activate Beclin-1-mediated autophagy, the Bcl-2/Bcl-xL-Beclin-1 complex must be dissociated, which can be accomplished by different mechanisms including competition for Bcl-2 binding by pro-apoptotic proteins with BH3 binding domains (e.g. Bid, Bad), c-Jun N-terminal kinase-1 (JNK1) phosphorylation of Bcl-2, or death-associated protein kinase (DAPK) phosphorylation of the BH3 domain of Beclin-1[15]. Beclin-1 also displays its dual roles in both autophagy and apoptosis as upon cleavage by caspases, Beclin-1 loses its autophagic potential and becomes a pro-apoptotic molecule that translocates to the mitochondria and facilitates cytochrome c release and caspase activation[36].

ATG5 is another protein that can play a role in both autophagic and apoptotic signaling. ATG5 is involved in the ATG12-ATG5-ATG16 complex which is vital for the formation of the autophagosome[37]. Additionally, research has shown that ATG5 can associate with Fas associated protein with death domain (FADD) and stimulate caspase-dependent apoptosis via the death receptor signaling pathway[38]. ATG5 is also associated with apoptosis as cleavage of ATG5 by calpains has been shown to lead to the translocation of cleaved ATG5 to the mitochondria where it interacts with Bcl-xL and causes pore formation, cytochrome c release, and subsequent caspase activation[39]. Similarly, ATG4D is a protein involved in the LC3 conjugation system, which upon cleavage by caspases will delipidate the LC3 homologue GABARAP-L1 causing a decrease in the number of GABARAP-L1 autophagosomes[33]. It has also been shown that caspase-cleaved

ATG4D translocates to the mitochondria, and that mitochondrial ATG4D increases the cells susceptibility to death, although the exact mechanism through which mitochondrial ATG4D contributes to cell death is unknown[40]. The role of ATG4D in cell death is further complicated by the fact that cleaved ATG4D localization to the mitochondria can be seen even in cells treated with caspase inhibitors, demonstrating that a pathway involving caspase-independent cleavage of ATG4D must also exist[40].

The interaction between autophagy and apoptosis can also be seen in cancer cells. In these cells, apoptotic pathways are usually impaired while autophagic pathways remain intact, leading to increased survival of these cells[41]. One mechanism responsible for this increased survival is the ability of autophagy to regulate apoptosis. In cancer cells known to be resistant to tumor necrosis factor-related apoptosis-inducing ligand (TRAIL)-mediated apoptosis (i.e. death receptor mediated apoptosis), caspase-8 is isolated within autophagosomes and then degraded by lysosomes, showing the ability of autophagy to inhibit apoptosis[41].

Clearly there is a considerable amount of interplay between the autophagic and apoptotic pathways. Further investigation of this interplay is warranted to better understand how these pathways regulate one another.

Apoptosis in skeletal muscle

Because of its unique multinucleated structure, skeletal muscle apoptosis is believed to occur differently than in mononucleated cells. While apoptosis normally results in death of the entire mononucleated cell, skeletal muscle is thought to undergo a specialized form of apoptosis known as “nuclear apoptosis”. During nuclear apoptosis, individual nuclei are said to be eliminated from the muscle fiber rather than death of the entire cell[42]. However, the idea of

nuclear apoptosis has been contested as of late as some studies have shown no myonuclear loss during skeletal muscle atrophy[43, 44]. Nevertheless, caspase and calpain activation in skeletal muscle can lead to cleavage of several muscle-specific substrates, resulting in atrophy and contractile dysfunction[45-47]. This suggests that nuclear apoptosis is not the only critical aspect of apoptotic signaling to consider in muscle pathogenesis.

Although apoptosis has been shown to be essential in the maintenance of mitotic cells, the role of apoptosis in post-mitotic tissues like skeletal muscle is less well understood[29]. Apoptotic signaling has been shown to be crucial in muscle differentiation, as the inhibition or deletion of caspase-3 in muscle cells causes a striking decrease in muscle fiber formation[48]. Conversely, apoptosis can also have detrimental effects in skeletal muscle. Increases in apoptosis along with muscle atrophy have been observed during immobilization, denervation, aging, and chronic heart failure[45, 49-51]. Skeletal muscle apoptosis is also initially increased after blunt crush injury, but eventually returns to basal levels[52]. Interestingly, suppressing apoptosis via caspase inhibition after this same blunt crush injury results in a faster restoration of muscle function[53]. Clearly, more research is needed to better understand the role of apoptosis in skeletal muscle homeostasis.

Autophagy in skeletal muscle

Nutrient deprivation is known to be a strong stimulator of autophagy in skeletal muscle[15]. However, there are also a variety of other stresses that can activate autophagy, including hypoxia, denervation, ER stress, oxidative stress, and mitochondrial damage[15]. In the absence of autophagy, increases in mitochondrial dysfunction, reactive oxygen species (ROS), ER stress, and atrophy-related gene expression (e.g. MurF-1, atrogin-1) have been observed, along with the

accumulation of ubiquitinated proteins and abnormal mitochondria[17, 54, 55]. Importantly, inhibition of autophagy has also been shown to cause DNA fragmentation, skeletal muscle atrophy, and decreased force production[17, 56]. These findings seem to suggest that autophagy plays a protective role in skeletal muscle homeostasis. However, other studies in skeletal muscle provide conflicting evidence regarding this topic. For example, increases in autophagy in combination with increased DNA fragmentation and muscle atrophy have been shown during muscle denervation[57]. Additionally, an upregulation of autophagy and DNA fragmentation has been observed in skeletal muscle after the injection of doxorubicin, a myotoxic drug[58]. A study by Mammucari and colleagues also found an upregulation of autophagy and muscle atrophy in mice expressing a constitutively active form of FoxO3 (i.e. a transcription factor that is necessary and sufficient to cause autophagy activation)[10]. Finally, a large increase in autophagy along with muscle weakness and premature death is observed during Pompe disease[56]. Due to these contradictory findings regarding the cytoprotective or cytotoxic role of autophagy, a more thorough investigation of autophagy in skeletal muscle is warranted.

Purpose

Because of the controversial role of autophagy in the protection against or induction of cell death mechanisms, it would be beneficial to examine the relationship between autophagic and apoptotic processes in greater detail. Specifically, due to the cell's ability to respond to various stresses by inducing autophagy, it is of interest to examine this relationship in skeletal muscle following muscle injury. To date, no research has examined if autophagy is directly involved in skeletal muscle damage and apoptosis, or if autophagy is required for skeletal muscle recovery after injury. Therefore, the purposes of this Master's thesis project were:

1) to examine the role of autophagy in modulating apoptotic signaling following cardiotoxin-induced skeletal muscle injury, and

2) to investigate the role of autophagy in skeletal muscle recovery after cardiotoxin-induced muscle damage.

To accomplish this, male skeletal muscle-specific inducible Atg7 knockdown (i.e. autophagy deficient) and wild-type control mice were studied.

Hypotheses

It was hypothesized that:

1) a post-developmental inhibition of autophagy will cause a greater increase in the initial apoptotic signaling in the skeletal muscle of the Atg7 knockdown compared to control mice in response to cardiotoxin-induced muscle damage (See Figure 1),

2) apoptotic signaling will remain elevated for a prolonged period of time during recovery in the Atg7 knockdown mice (See Figure 1), and

3) a reduction in muscle regeneration will be observed in the Atg7 knockdown mice as evidenced by a greater difference in fiber cross-sectional area between day 0 and day 14 in the Atg7 knockdown mice compared to control mice (See Figure 2). Additionally, it is hypothesized that the proportion of the muscle containing damaged and/or centrally nucleated (i.e. regenerating) fibers will be elevated in the knockdown animals relative to the control animals on day 14.

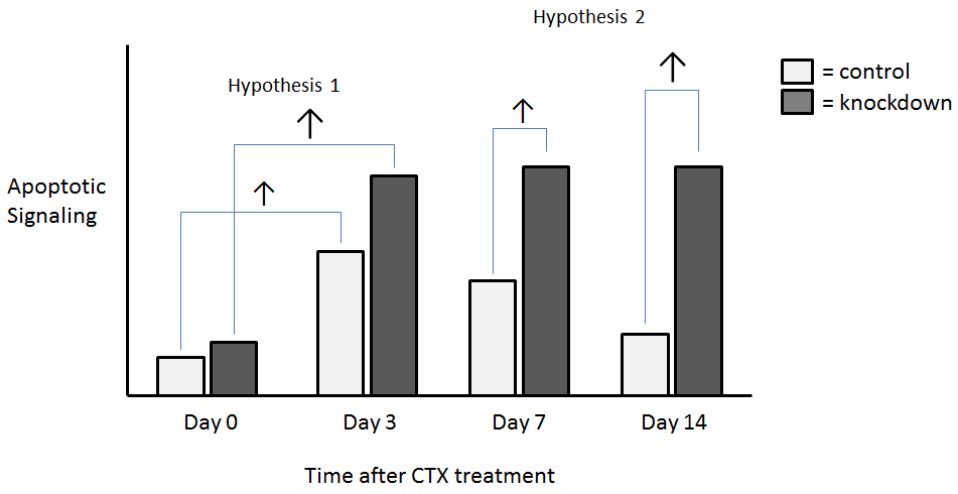

Figure 1: Visual representation of hypothesis 1 and 2. The response observed between day 0 and day 3 was considered the "muscle damage" phase, while the response seen on day 7 and day 14 was considered the "muscle recovery" phase.

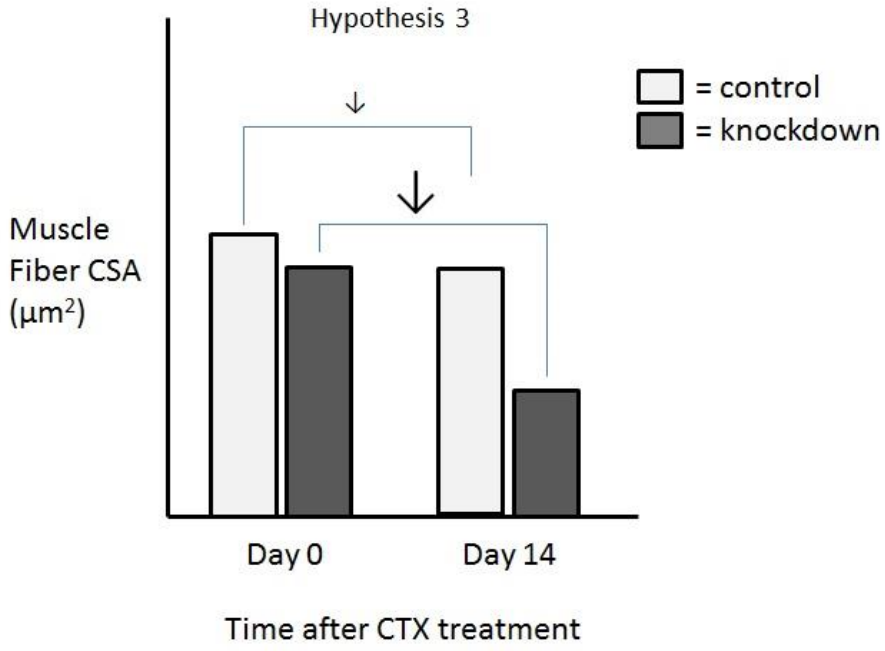

Figure 2: Visual representation of hypothesis 3.

It was hypothesized that these changes would occur because upon muscle injury, a variety of organelles and proteins would become damaged and would accumulate due to a lack of autophagy in the Atg7 knockdown mice. This accumulation would lead to further damage, activation of apoptotic signaling, and fiber atrophy. These changes would provide support for the idea that autophagy serves a cytoprotective role in skeletal muscle and would further elucidate the relationship between autophagy and apoptosis.

Methods

Animals

The animals used in this study were generated by first breeding Atg7 F/F mice (kindly donated by Herbert Virgin, Washington University)[18] with HSA-MerCreMer mice (kindly donated by Karyn Esser, University of Kentucky)[59]. The Atg7 F/F animals contain Atg7 genes that are flanked by LoxP sites (i.e. floxed) on both chromosomes, meaning they are homozygous for the "floxed" gene. These LoxP sites are specific 34 base pair sequences that must be inserted into the mouse genome through transgenic technology as they are not normally found in mouse DNA[60]. The HSA-MerCreMer animals express the wild-type (WT) Atg7 gene on both chromosomes (i.e. rather than the "floxed" Atg7gene), but are also hemizygous for the Cre recombinase (Cre) gene. The importance of the Cre gene is that when it is transcribed and translated to form the Cre recombinase enzyme, and this enzyme is present in the nucleus, it is able to recognize and bind to LoxP sites[60]. The enzyme then catalyzes the recombination of the genes between the LoxP sites, rendering these genes useless[60]. In turn, if an animal expresses floxed Atg7 genes, and Cre recombinase is present in the nucleus, the Atg7 genes will be removed resulting in the production of Atg7 knockdown mice. Due to the important role of ATG7 in autophagosome formation, knocking out this gene will produce mice that are autophagy deficient. In our model, the Cre gene is surrounded by two mutated estrogen receptor (Mer) ligand binding domains that have a 1000-fold lower affinity to estrogen[61, 62], yet maintain their affinity for the synthetic compound 4-hydroxytamoxifen (herein referred to simply as tamoxifen). This gene complex is also connected to the promoter and first exon of the human α-skeletal actin (HSA) gene, thereby regulating Cre expression in a skeletal muscle-specific manner[63].

Although the Mutated estrogen receptor-Cre recombinase-Mutated estrogen receptor (MerCreMer) protein complex is transcribed whenever the HSA promoter is activated, this model is considered inducible because in the absence of tamoxifen, this complex remains in the cytosol. In turn, the Cre recombinase enzyme does not have access to the LoxP sites surrounding the Atg7 genes and the genes remain intact[64, 65]. However, when animals that express the Cre gene as well as floxed Atg7 genes are injected with tamoxifen, the tamoxifen will bind to the Mer ligand binding domains and cause a translocation of the MerCreMer complex into the nucleus[64, 65]. Once in the nucleus, Cre recombinase will bind to the LoxP sites and cause recombination of the Atg7 genes[64, 65].

The offspring produced by crossing the Atg7 F/F and HSA-MerCreMer mice were either Atg7 F/WT or Atg7 F/WT^{Cre}. The Atg7 F/WT^{Cre} mice were then used in the next breeding step, where they were bred back to the Atg7 F/F mice. This resulted in the birth of 4 different groups of mice: Atg7 F/WT mice which were sacrificed, Atg7 F/WT^{Cre} mice which were used for subsequent breeding, Atg7 F/F mice which were used as control animals, and Atg7 F/F^{Cre} mice which were used as the inducible Atg7 knockdown mice.

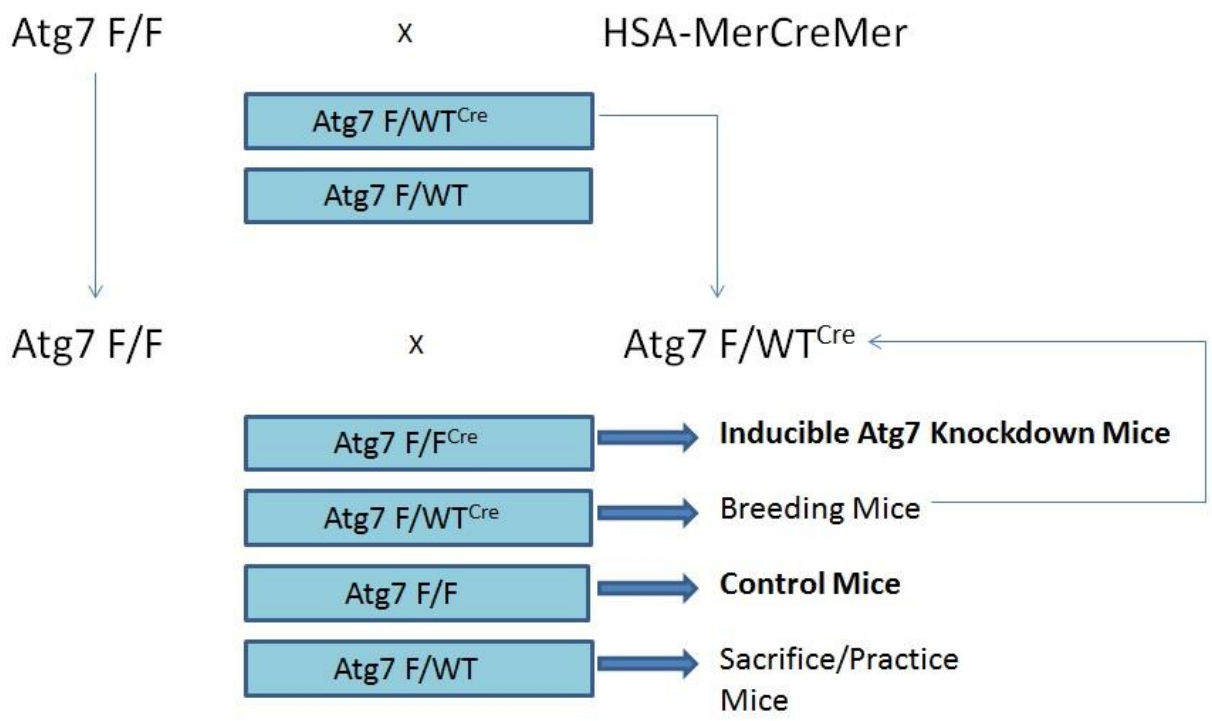

Figure 3: Breeding diagram. The Atg7 F/F^{Cre} mice produced by crossing the Atg7 F/F and Atg7 F/Wt^{Cre} in the second breeding step were used as the experimental mice (i.e. as the inducible Atg7 knockdown mice), while the Atg7 F/F mice produced from the same breeding combination were used as the control mice.

Experimental design

First, Atg7 F/F^{Cre} mice were given intraperitoneal injections of tamoxifen (Atg7 F/F^{Cre}+Tam) for 5 consecutive days in order to stimulate transcription of the Cre recombinase enzyme to promote Atg7 knockdown. Atg7 F/F mice were also injected with tamoxifen at this time point (Atg7 F/F+Tam). After a 2-week period to allow for significant Atg7 knockdown in the Atg7 F/F^{Cre}+Tam animals[66] (pilot studies revealed a reduction of ~55-70% in soleus and plantaris ATG7 protein, while no reduction was seen in heart or liver; Appendix figure A1), these mice received intramuscular injections of cardiotoxin (CTX) into the tibialis anterior, as well as both heads of the gastrocnemius on both legs (i.e. 3 injections per leg, 6 injections total)

(Atg7 F/F^{Cre}+Tam+CTX). The Atg7 F/F mice were also injected with CTX at this point in time (Atg7 F/F+Tam+CTX). Cardiotoxin injections were performed to allow us to examine the physiological response to muscle injury as CTX is a myotoxic compound that induces rapid muscle fiber depolarization and contraction that leads to plasma membrane disruption and fiber lysis[2]. Ultimately, this experimental design produced 2 groups:

Group 1= Atg7 F/F^{Cre}+Tam+CTX

Group 2 = Atg7 F/F+Tam+CTX

Animals from each group were sacrificed 0, 3, 7, and 14 days after cardiotoxin injection (Note: day 0 animals were sacrificed after the 2 week washout period without receiving cardiotoxin injections). These time points were chosen to allow us to examine various cellular features prior to muscle injury (i.e. day 0), during the inflammatory phase of injury (i.e. day 3), during the muscle fiber regeneration phase (i.e. day 7), and after the muscle had regenerated intact fibers and regained a relatively normal muscle architecture (i.e. day 14)[2]. Autophagic, apoptotic, and morphological data was collected using immunoblotting, caspase, calpain, cathepsin, and proteasome activity assays, ROS production assays, immunohistochemical fiber type staining, and hematoxylin and eosin (H & E) staining.

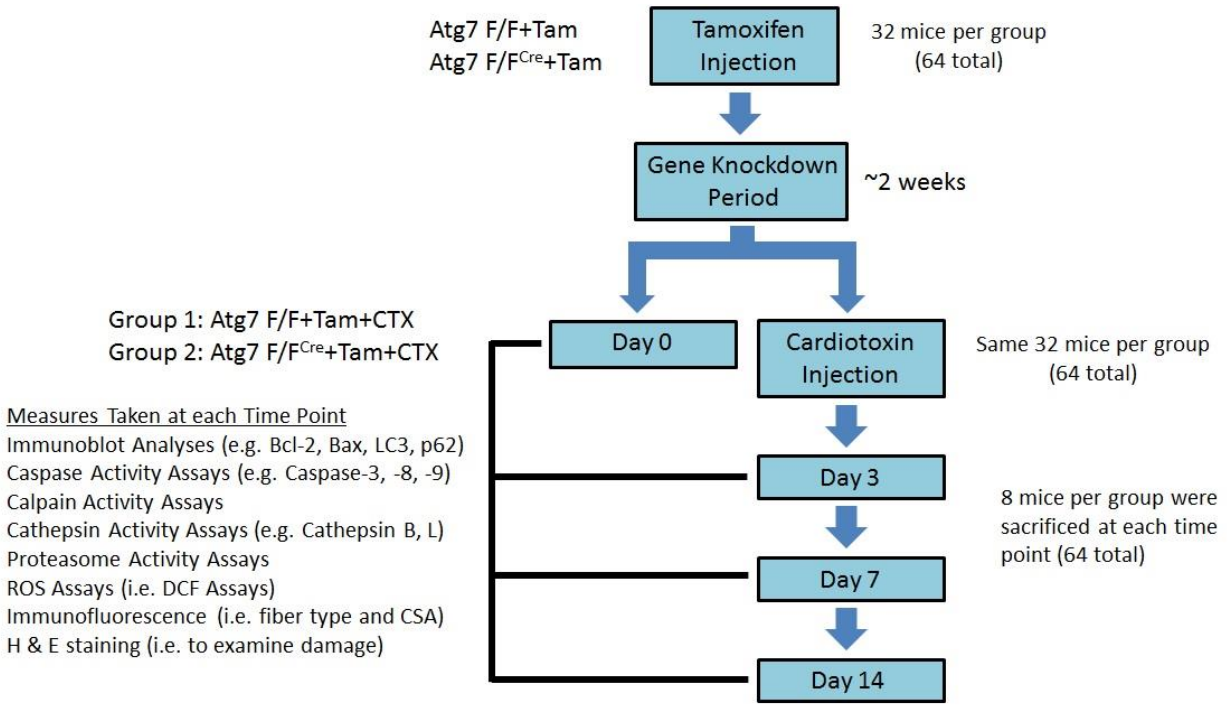

Figure 4: Experimental design. Both the F/F and F/F^{Cre} mice received tamoxifen injections for 5 consecutive days. This injection period was followed by a 2 week period to allow for gene knockdown. After this, some mice from both groups were sacrificed and classified as day 0 mice, while additional animals received intramuscular injections of cardiotoxin. Animals from both the F/F and F/F^{Cre} groups were sacrificed 3, 7, and 14 days post-cardiotoxin injections.

Tamoxifen and cardiotoxin injections

Nine to twelve week old Atg7 F/F and Atg7 F/F^{Cre} mice were injected (i.e. via intraperitoneal injection) with 2 mg of tamoxifen dissolved in sunflower seed oil (10mg/mL) daily for 5 days. Pilot data was collected to ensure that this dose effectively knocked down the Atg7 gene in the Atg7 F/F^{Cre} mice (Appendix Figure A1).

After a 2 week period to allow for significant recombination of the Atg7 gene, the Atg7 F/F and Atg7 F/F^{Cre} animals that were injected with tamoxifen were anaesthetized using isoflurane and given a 50µL intramuscular injection of 10µM cardiotoxin (Naja mossambica mossambica; Sigma-Aldrich, product #: C9759) into the tibialis anterior, and a 75µL injection

into each head of the gastrocnemius in both legs (i.e. 3 cardiotoxin injections per leg, 6 total). All mice received a 60 µL subcutaneous injection of meloxicam (i.e. a non-steroidal anti-inflammatory drug with analgesic effects) immediately after and 24 hours post-cardiotoxin treatment.

Muscle extraction and sample preparation

Mice were sacrificed by cervical dislocation at day 0 (i.e. prior to cardiotoxin injection), and 3, 7, and 14 days after cardiotoxin injection. The tibialis anterior (TA) was extracted from both legs: one was frozen in liquid nitrogen, while a sample of the entire circumference from the middle portion of the other TA was embedded in Optimal Cutting Temperature (OCT) compound (Tissue-Tek) and frozen in liquid nitrogen-cooled isopentane. These samples were then stored at -80°C. The gastrocnemius was also removed from each leg and was first separated into its two heads, and then each head was separated in half with equal portions of red and white gastrocnemius. These muscle samples were then frozen in liquid nitrogen by freeze clamping and stored at -80°C. Lastly, soleus and plantaris muscles were extracted at all time points, and quadriceps muscle was isolated on day 14. These muscles were frozen in liquid nitrogen and stored at -80°C.

Gastrocnemius and quadriceps muscle samples to be used for immunoblotting were homogenized in ice-cold lysis buffer (20mM HEPES, 10mM NaCl, 1.5mM $MgCl_2$, 1mM DTT, 20% glycerol and 0.1% Triton X-100; pH 7.4) that included protease inhibitors (Complete Cocktail; Roche Diagnostics) using a handheld glass homogenizer. Gastrocnemius muscle samples to be used for caspase, calpain, cathepsin, and proteasome activity assays were homogenized in a similar manner in the absence of protease inhibitors. Homogenates were

centrifuged at 1000g for 10 minutes at 4°C and the supernatants were collected and stored at -80°C. Protein concentration of the supernatants was determined by BCA protein assay.

Immunoblot analyses

For immunoblotting, equal amounts of protein from gastrocnemius homogenates were loaded into 12% SDS-PAGE gels and separated by electrophoresis. Proteins were transferred onto PVDF membranes (BioRad) which were then blocked at 4°C overnight or at room temperature for 1 hour using 5% (w/v) milk-TBST. Blocked membranes were incubated in primary antibody at 4°C overnight or at room temperature for 1 hour. After primary antibody incubation, the membranes were washed with TBST and incubated with an appropriate horseradish peroxidise-conjugated secondary antibody (Santa Cruz Biotechnology) at room temperature for 1 hour. The proteins were then imaged using Clarity™ Western ECL Substrate (BioRad) or ECL Western Blot Substrate (BioVision) and the ChemiGenius 2 Bio-Imaging System (Syngene). The optical densities of the imaged bands were analyzed using GeneTools software (Syngene). A standard muscle sample of known protein concentration was also loaded into each SDS-PAGE gel to allow for normalization of the results. Finally, to guarantee equal protein loading and quality of protein transfer, membranes were stained with Ponceau S (Sigma-Aldrich).

Immunoblots were conducted with primary antibodies against ATG7 (1:500; product #: 8558), LC3B (1:500; product #: 2775), Beclin-1 (1:1000; product #: 3738), ATG4B (1:1000; product #: 5299) [Cell Signaling], p62 (1:500; product #: GP62-N) [Progen], Hsp70 (1:2000; product #: ADI-SPA-810), XIAP (1:1000; product #: ALX-210-327), MnSOD (1:7500; product #: ADI-SOD-110), CuZnSOD (1:2000; product #: ADI-SOD-101) [Enzo Life Sciences], catalase

(1:2000; product #: 219010) [EMD Millipore], cytochrome c (1:2000; product #: sc-13156), Bcl-2 (1:200; product #: sc-7382), Bax (1:1000; product #: sc-493), Bid (1:500; product #: sc-11423), MAFbx (1:200; product #: sc-33782), and MuRF1 (1:200; product #: sc-32920) [Santa Cruz Biotechnology].

Caspase and calpain enzyme activity

The activity of caspase-3, caspase-8, and caspase-9 in gastrocnemius muscle homogenates was measured using the substrates Ac-DEVD-AFC (Enzo Life Sciences, product #: ALX-260-032), Ac-IETD-AMC (Sigma-Aldrich, product #: A4188), and Ac-LEHD-AMC (Enzo Life Sciences, product#: ALX-260-080), respectively. In their pro form, these substrates emit only low levels of fluorescence, but upon proteolytic cleavage by their respective active caspase enzyme they produce highly fluorescent products[67]. Muscle samples were incubated (in duplicate) in assay buffer (20mM HEPES, 10% glycerol, 10mM DTT) with Ac-DEVD-AFC, Ac-IETD-AMC, or Ac-LEHD-AMC at room temperature for 2 hours in black 96-well plates. A Synergy H1 multi-mode microplate reader (Biotek) was then used to measure fluorescence with excitation and emission wavelengths of 360 nm and 440 nm, respectively. Enzyme activity of caspase-3, caspase-8, and caspase-9 was normalized to total protein content and the fluorescence intensity was expressed in arbitrary units per milligram protein.

For calpain activity, gastrocnemius samples were incubated in duplicate at 30˚C for 2 hours in assay buffer (20mM HEPES, 10% glycerol, 10mM DTT) with Suc-LLVY-AMC (Enzo Life Sciences, product #: BML-P802) in black 96-well plates. One additional well also contained the homogenate, Suc-LLVY-AMC, and the calpain inhibitor Z-LL-CHO (Enzo Life Sciences). A Synergy H1 multi-mode microplate reader (Biotek) was used to measure fluorescence with

excitation and emission wavelengths of 360 nm and 440 nm, respectively. Calpain activity was calculated by subtracting the fluorescence of the well with the inhibitor from the average fluorescence of the wells without the inhibitor. This value was then normalized to total protein content and expressed as fluorescence intensity in arbitrary units per milligram protein.

Cathepsin activity

Activity of lysosomal enzymes was measured through the use of the fluorogenic substrate z-FR-AFC (Enzo Life Sciences, product #: ALX-260-129), which is considered to indicate cathepsin L and B activities[68, 69]. Gastrocnemius homogenates were loaded into assay buffer (50 mM sodium acetate, 8 mM DTT, 4 mM EDTA, 1 mM Pefabloc; pH 5.0) in duplicate in black 96-well plates. The z-FR-AFC substrate was then added to produce an in-well concentration of 50 µM, and the plate was warmed at 30°C for 5 minutes. To measure fluorescence, a Synergy H1 multi-mode microplate reader (Biotek) was used with excitation and emission wavelengths of 400 nm and 505 nm, respectively, for 30 minutes at 30°C. Cathepsin activity was normalized to total protein content and expressed as fluorescence intensity in arbitrary units per milligram of protein.

Proteasome activity

The fluorogenic substrate Suc-LLVY-AMC (Enzo Life Sciences, product #: BML-P802) was used to examine chymotrypsin-like activity of the proteasome[70]. Gastrocnemius samples were incubated in assay buffer (50 mM Tris/HCl, 25 mM KCl, 10 mM NaCl, 1 mM $MgCl_2$; pH 7.5) in the dark at 30°C for 1 hour with substrate, or with a combination of substrate and the proteasome inhibitor epoxomicin (Cayman Chemical, product #: 10007806) in black 96-well plates. Fluorescence was measured using a Synergy H1 multi-mode microplate reader (Biotek)

with excitation and emission wavelengths of 360nm and 460nm, respectively. Proteasome activity was then determined by taking the difference between samples incubated with and without the proteasome inhibitor, and values were normalized to protein content and expressed as fluorescence intensity using arbitrary units per milligram of protein.

Reactive oxygen species (ROS) generation

Whole muscle reactive oxygen species production was examined using dichlorofluorescein-diacetate (DCFH-DA) (Life Technologies, product #: C6827). Intracellular esterases hydrolyze DCFH-DA which leads to the formation of non-fluorescent DCFH. DCFH can be oxidized by various reactive oxygen species to generate DCF, a highly fluorescent molecule. Homogenization of gastrocnemius muscle samples was performed in ice-cold lysis buffer (250mM sucrose, 20 mM HEPES, 10 mM KCl, 1 mM EDTA, 1mM EGTA, 1mM DTT; pH 7.4) containing protease inhibitors (Complete Cocktail; Roche Diagnostics) in a handheld glass homogenizer. After this, the gastrocnemius samples were loaded in duplicate with 5 μM DCFH-DA and were subsequently incubated at 37°C in the dark for 1 hour in black 96-well plates. A Synergy H1 multi-mode microplate reader (Biotek) with excitation and emission wavelengths of 490 nm and 525 nm, respectively, was then used to quantify fluorescence. The intensity of the measured fluorescence was normalized to total protein content and presented as arbitrary units per milligram of protein.

Immunofluorescence

Tibialis anterior muscle samples embedded in OCT compound were cut using a cryostat (Thermo Scientific) maintained at -20°C into 10μm cross-sections and were then stored at -80°C. Prior to staining, slides were air dried for 10 minutes (Note: this was done at room temperature

as were all of the following steps). After this, slides were blocked with 10% goat serum in 1x PBS for 1 hour. Primary antibodies against myosin heavy chain (MHC) I (BA-F8; 1:25), MHCIIa (SC-71; 1:500), MHCIIb (BF-F3; 1:50), and dystrophin (MANDYS1[3B7]; 1:100) (Developmental Studies Hybridoma Bank) were then applied overnight in order to identify myosin heavy chain and dystrophin expression. Next, slides were washed 3 times for 5 minutes in 1x PBS, and anti-mouse isotype-specific secondary antibodies (Life Technologies) were applied for 2 hours. Slides were once again washed 3 times for 5 minutes in 1x PBS, and a #1 coverslip was mounted on each slide with Prolong Gold antifade reagent. Imaging was performed the following day using an Axio Observer Z1 fluorescent microscope equipped with an AxioCam HRm camera and associated AxioVision software (Carl Zeiss). Quantitative data for fiber type composition was obtained by counting all fibers within a muscle section, and fiber type-specific CSA was determined by outlining fibers from 5 separate regions of each cross section (30 fibers per muscle fiber type). Whole muscle CSA was determined by outlining the entire muscle cross-section.

Note: Primary and secondary antibody cocktails were prepared in blocking solution (i.e. 10% goat serum in 1x phosphate-buffered saline [PBS]). The anti-mouse isotype-specific secondary antibody used for MHCI was Alexa Fluor 350 IgG2b (blue; 1:500), for MHCIIa was Alexa Fluor 488 IgG1 (green; 1:500), for MHCIIb was Alexa Fluor 555 IgM (red; 1:500), and for dystrophin was Alexa Fluor 555 IgG2a (red; 1:500).

Hematoxylin & Eosin (H & E) staining

Tibialis anterior muscle cross-sections mounted on microscope slides were first stained with hematoxylin for 30 seconds, after which excess hematoxylin was quickly removed. The slides were then dipped in distilled water 5 times. After repeating the previous step two more

times, cross-sections were stained with eosin for 90 seconds, after which excess eosin was quickly removed. Slides were then dipped in 70% ethanol 5 times, 95% ethanol 5 times, and 100% ethanol 5 times, with excess ethanol being quickly removed between each percentage of alcohol. The previous step was repeated one more time. Finally, slides were dipped 5 times in xylene, the excess was removed, and permount was applied to mount a #1 coverslip.

Muscle damage was quantified on day 3, 7, and 14 by circling the area of the TA cross-sections occupied by fibers that had visible morphological damage or centralized nuclei. This damaged area was then converted into a percentage of the total muscle cross-sectional area.

Statistical analyses

Statistical analysis of day 0 protein expression and weight data was performed using Student's t-tests. Analysis of ATG7 protein content in undamaged quadriceps on day 14 was also performed using Student's t-tests.

Protein expression, enzyme activity, and ROS generation data obtained across the 14 day study period was analyzed using a 2-way analysis of variance (ANOVA) and Bonferroni post hoc testing, where genotype (2 levels) and time (4 levels) represented the independent variables in the ANOVA. Data regarding the proportion of muscle damage was analyzed on day 3, 7, and 14 by 2-way ANOVA and Bonferroni post hoc tests, where genotype (2 levels) and time (3 levels) represented the independent variables in the ANOVA. Fiber type distribution, total fiber number, fiber type-specific cross-sectional area, and whole muscle cross-sectional area data was analyzed on day 0 and 14 using a 2-way ANOVA, where genotype (2 levels) and time (2 levels) represented the independent variables. Bonferroni post hoc tests were also conducted if any main

effects were discovered. For all tests, $p<0.05$ was considered statistically significant, while $0.10 \geq p \geq 0.05$ was considered a trend towards significance.

Results

Atg7 knockdown on day 0 and the resultant effect on key autophagic markers, body weight, and muscle weights

Immunoblot analyses of gastrocnemius homogenates from day 0 mice revealed a reduction of ~61% ($p<0.05$) in ATG7 protein content in F/F^{Cre} compared to F/F mice (Figure 5A). While no significant changes in p62 (Figure 5B) or LC3B-I (Figure 5C) expression were observed, a trend ($p=0.10$) towards decreased LC3B-II (Figure 5D) and a significant decrease ($p<0.05$) in the LC3B-II:I ratio (Figure 5E) was seen in the F/F^{Cre} animals.

A trend ($p=0.10$) towards significantly lower body weight was discovered in the F/F^{Cre} group relative to the F/F group on day 0 (Figure 6A). Additionally, a significant reduction ($p<0.05$) in absolute muscle weight was observed in the TA (Figure 6B), gastrocnemius (Figure 6C), and plantaris (Figure 6D) of the F/F^{Cre} mice compared to the F/F mice. Conversely, absolute soleus muscle weight (Figure 6E) was found to be similar between groups.

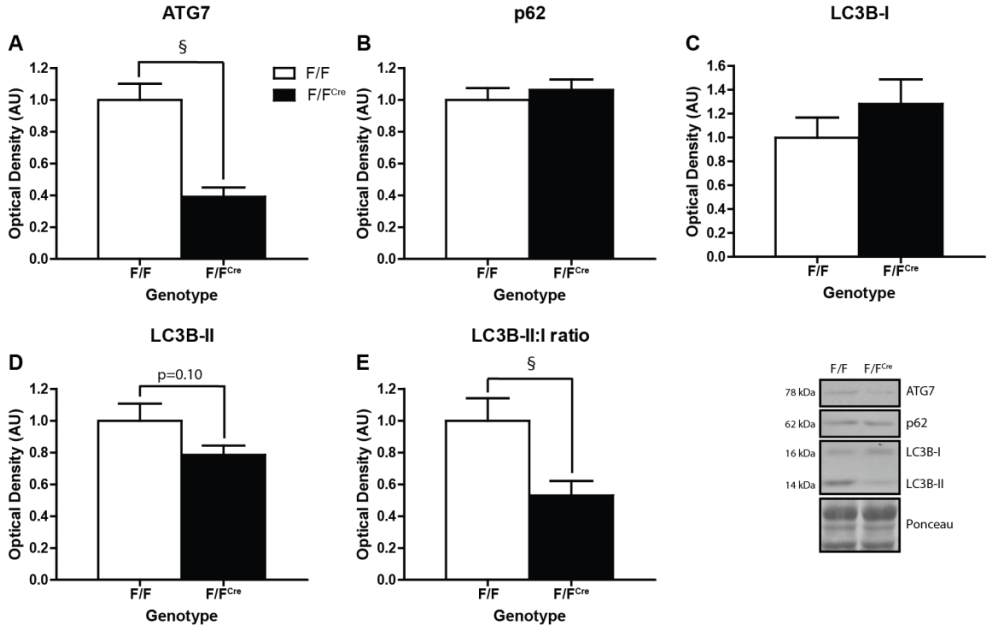

Figure 5: Examination of Atg7 knockdown on day 0 and the resultant effect on key autophagic proteins. Quantitative analysis of ATG7 (A), p62 (B), LC3B-I (C), LC3B-II (D), and the LC3B-II:I ratio (E) in the gastrocnemius (n=8 per group), along with representative immunoblots of each protein. § significant difference between indicated bars as determined by Student's t-test.

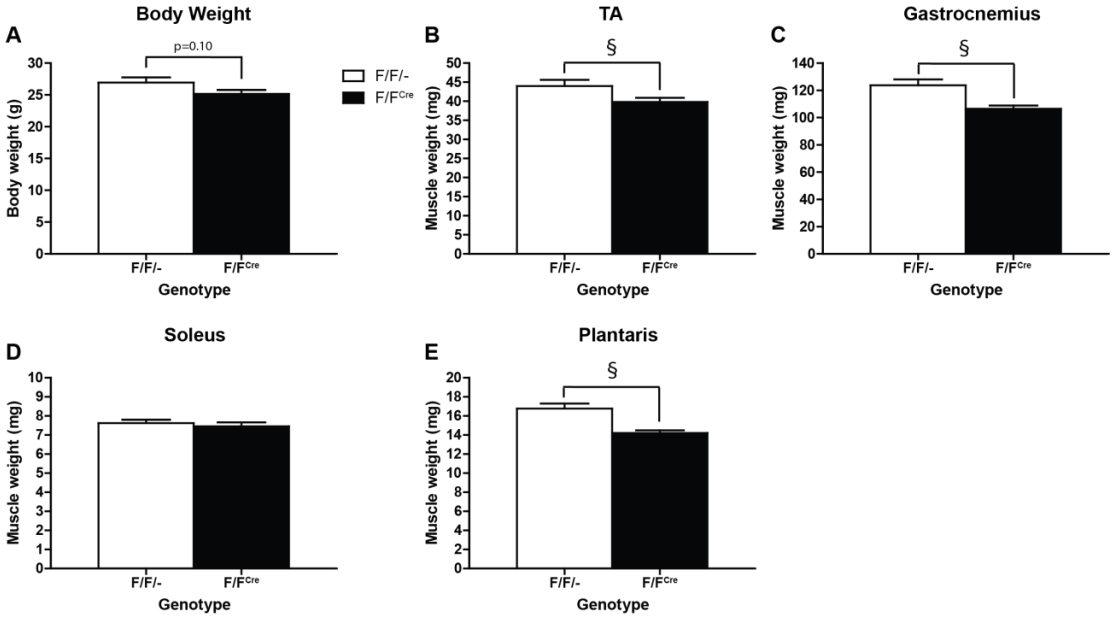

Figure 6: Body weight and absolute muscle weights on day 0. Quantification of body weight (A), absolute TA (B), gastrocnemius (C), soleus (D), and plantaris (E) muscle weights (n=8 per group). § significant difference between indicated bars as determined by Student's t-test.

Body and normalized muscle weights after cardiotoxin injection

A main effect of genotype ($p<0.05$) was found for body weight (BW), with the F/F^{Cre} mice showing a lower average BW over the study period compared to the F/F mice (Figure 7A). A main effect of genotype ($p<0.05$) was also seen when assessing tibialis anterior weight normalized to body weight, with the F/F^{Cre} animals showing higher average TA weight/BW over the study period (Figure 7B). Additionally, a main effect of time ($p<0.05$) was found with post hoc tests revealing increased TA weight/BW on day 3 compared to all other days (Figure 7B). Finally, a main effect of time ($p<0.05$) was found for gastrocnemius weight normalized to body weight, with post hoc tests showing increased gastrocnemius weight/BW on day 3 compared to all other days, and on day 0 relative to day 7 and 14 (Figure 7C).

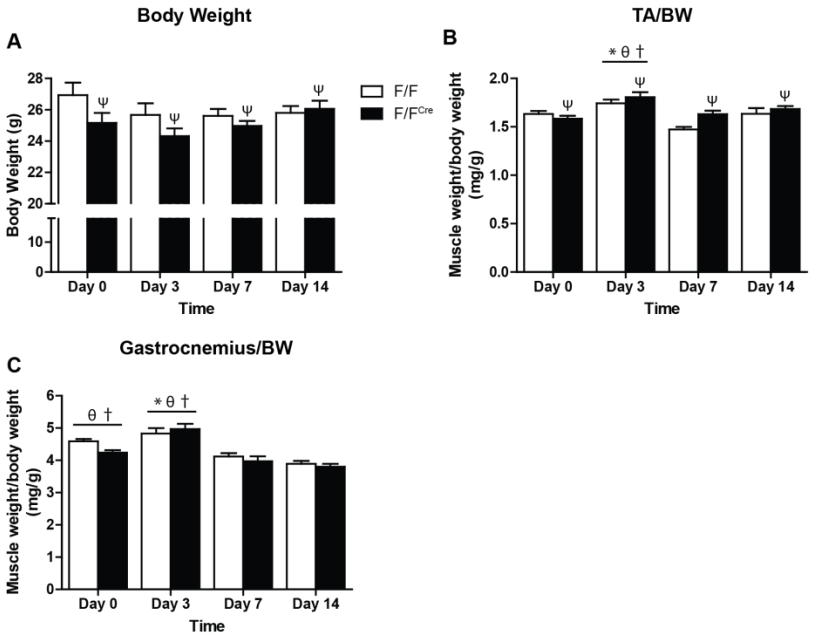

Figure 7: Body weight and normalized muscle weights after cardiotoxin injection. Quantification of body weight (A), tibialis anterior weight normalized to body weight (B), and gastrocnemius weight normalized to body weight (C) over the 14 day study period (n=8 per group). Note: day 0 values presented in this figure for body weight are the same as those presented in Figure 6. Ψ significant difference compared to F/F (main effect). * significant difference compared to day 0 (main effect). θ significant difference compared to day 7 (main effect). † significant difference compared to day 14 (main effect).

Autophagic protein expression and cathepsin activity in gastrocnemius after cardiotoxin exposure

A significant interaction effect ($p<0.05$) was observed for ATG7 expression across the study period (Figure 8A). Post hoc tests revealed no significant differences between groups at any of the studied time points. Within genotypes, both groups showed lower ATG7 expression on day 0 compared to all other days. Additionally, the F/F group showed similar ATG7 content on days 3, 7, and 14. Alternatively, while the F/F^{Cre} animals showed similar ATG7 protein levels on day 3 compared to day 7, and on day 7 compared to 14, a significant increase in ATG7 content on day 3 relative to day 14 was observed. A significant main effect of time ($p<0.05$) was observed for p62, with higher levels of p62 expression on both day 0 and day 14 compared to day 3 and 7, and day 7 expression being greater than that on day 3 (Figure 8B). A trend ($p=0.08$) towards a genotype effect of higher p62 expression in the F/F^{Cre} animals was also observed (statistical trend not noted on graph). LC3B-I protein content also showed a main effect of time ($p<0.05$), with increased levels on day 7 compared to all other time points (Figure 8C). A main effect of time ($p<0.05$) was seen for LC3B-II as well, with post hoc tests showing increased content on all days compared to day 0, and on day 7 and 14 relative to day 3 (Figure 8D). Finally, a main effect of time ($p<0.05$) was found for the LC3B-II:I ratio, with day 14 showing a higher ratio than all other days (Figure 8E).

A significant main effect of time ($p<0.05$) was observed for Beclin-1, with increased expression being seen on day 7 compared to all other days, while day 3 and 14 showed increased expression compared to day 0 (Figure 8F). A trend ($p=0.08$) towards higher Beclin-1 content on day 3 compared to day 14 was also observed (statistical trend not noted on graph). Analysis of ATG4B content also showed a main effect of time ($p<0.05$), with post hoc tests revealing

increased expression at all time points compared to day 0, and increased expression on day 3 and 7 relative to day 14 (Figure 8G).

Finally, a main effect of time ($p<0.05$) was seen for cathepsin activity, with post hoc tests showing higher activity on day 3, 7, and 14 compared to day 0, on day 3 compared to day 7 and 14, and on day 7 compared to day 14 (Figure 12F).

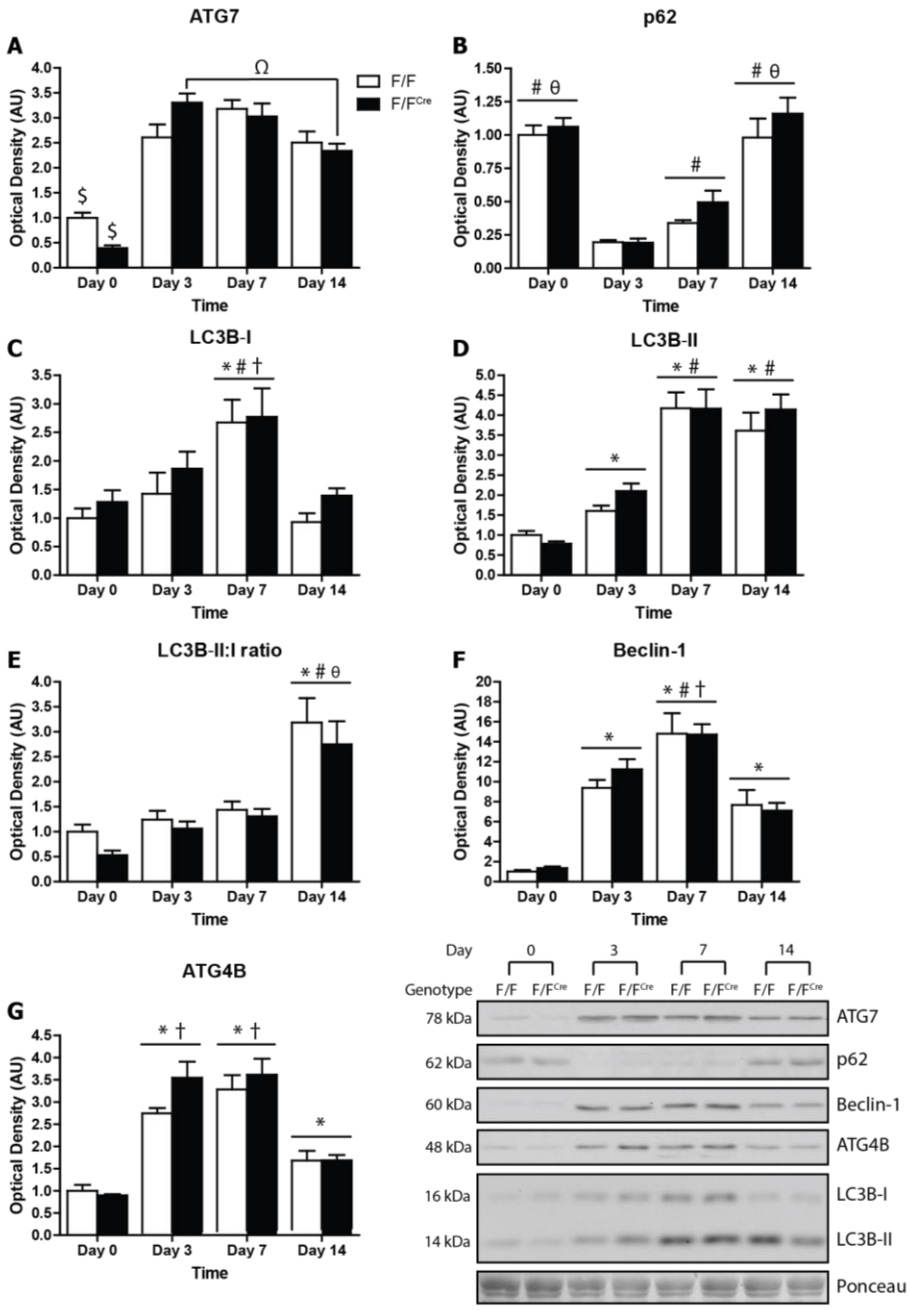

Figure 8: Autophagic protein expression over the course of the 14 day study period. Quantitative analysis of ATG7 (A), p62 (B), LC3B-I (C), LC3B-II (D), LC3B-II:I ratio (E), Beclin-1 (F), and ATG4B (G) in the gastrocnemius (n=8 per group), along with representative immunoblots of each protein. Note: day 0 values presented in this figure for ATG7, p62, LC3B-I, LC3B-II, LC3B-II:I ratio are the same as those presented in Figure 5. $ significant difference within genotype compared to day 3, 7, and 14 (interaction effect). Ω significant difference between indicated bars (interaction effect). * significant difference compared to day 0 (main effect). # significant difference compared to day 3 (main effect). θ significant difference compared to day 7 (main effect). † significant difference compared to day 14 (main effect).

ATG7 protein content on day 14 in undamaged quadriceps muscle

Due to the increase in ATG7 protein beyond day 0 in the cardiotoxin-damaged gastrocnemius muscle of the F/F^{Cre} mice, we decided to examine whether the return of ATG7 was an effect of time or whether it was an effect of the muscle being damaged as a result of cardiotoxin exposure. To validate our knockdown model and prove that the recovery of ATG7 expression was not simply an effect of time (i.e. to prove that our knockdown lasted longer than the study period), we examined the expression of ATG7 between groups in undamaged quadriceps muscle on day 14. Significantly lower ($p<0.05$) ATG7 protein content was observed between groups, with a reduction of ~87% seen in the F/F^{Cre} compared to the F/F animals (Figure 9). This result proved that the return of ATG7 protein in the F/F^{Cre} mice was not simply an effect of time.

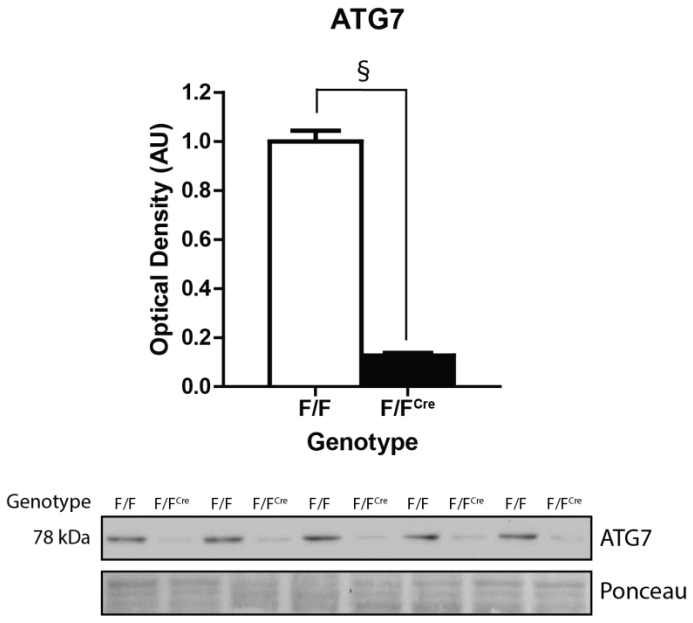

Figure 9: Quantitative analysis of ATG7 protein content on day 14 in undamaged quadriceps muscle. A representative immunoblot is also provided (n=5 per group). Means for each group are presented relative to the F/F group. § significant difference between the indicated bars as determined by Student's t-test.

Ubiquitin-proteasome related protein expression and proteasome activity in gastrocnemius post-cardiotoxin injection

A significant main effect of time ($p<0.05$) was seen for both MAFbx (Figure 10A) and MuRF1 (Figure 10B) protein expression in the gastrocnemius, with post hoc tests showing lower levels on day 3, 7, and 14 compared to day 0, and increased levels on day 14 relative to day 3 and 7. Post hoc analysis of MuRF1 also showed a trend ($p=0.10$) towards increased expression on day 7 compared to day 3.

A main effect of time ($p<0.05$) was also seen for proteasome activity in the gastrocnemius, with higher activity being observed on both day 7 and day 14 compared to day 0 and day 3 (Figure 12F).

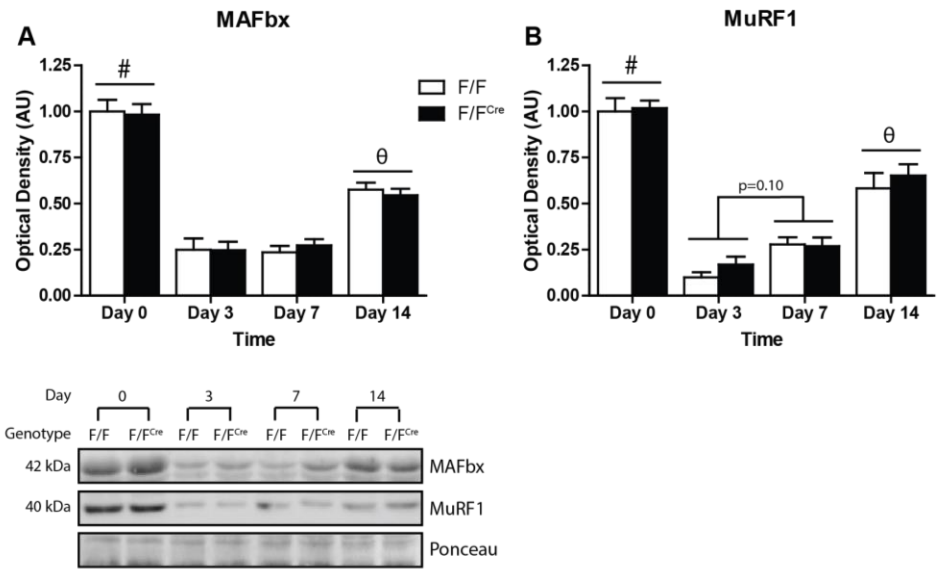

Figure 10: Ubiquitin-proteasome related protein expression over the 14 day study period. Quantitative analysis of MAFbx (A) and MuRF1 (B) in the gastrocnemius (n=8 per group), along with representative immunoblots of each protein. # significant difference compared to day, 3, 7, and 14 (main effect). θ significant difference compared to day 3 and 7 (main effect).

Expression of apoptotic proteins in gastrocnemius in response to cardiotoxin exposure

A significant main effect of time ($p<0.05$) was discovered for Bax, with higher expression observed on day 3 and 7 compared to day 0 and 14 (Figure 11A). Bcl-2 also showed a main effect of time ($p<0.05$), with post hoc tests revealing increased Bcl-2 content on day 3, 7, and 14 compared to day 0, along with increased expression on day 3 and 7 relative to day 14 (Figure 11B). Interestingly, no effects were observed for the Bax:Bcl-2 ratio (Figure 11C). A significant main effect of time ($p<0.05$) was seen for Bid, with higher expression seen on day 3 compared to day 0 and 14, and on day 7 compared to day 0 (Figure 11D). A significant time effect ($p<0.05$) was also observed for tBid, as post hoc tests showed higher levels on day 0 and 14 relative to day 3 and 7 (Figure 11E). These results contributed to a main effect of time ($p<0.05$) for the tBid:Bid ratio, with post hoc tests revealing an increased ratio on day 0 compared to all other days, and on day 14 compared to day 3 and 7 (Figure 11F). Finally, XIAP expression also showed a significant main effect of time ($p<0.05$), with higher expression observed on day 3, 7 and 14 relative to day 0, and on day 3 compared to day 14 (Figure 11G). A strong trend ($p=0.05$) towards higher XIAP levels on day 7 relative to day 14 was also discovered (statistical trend not noted on graph).

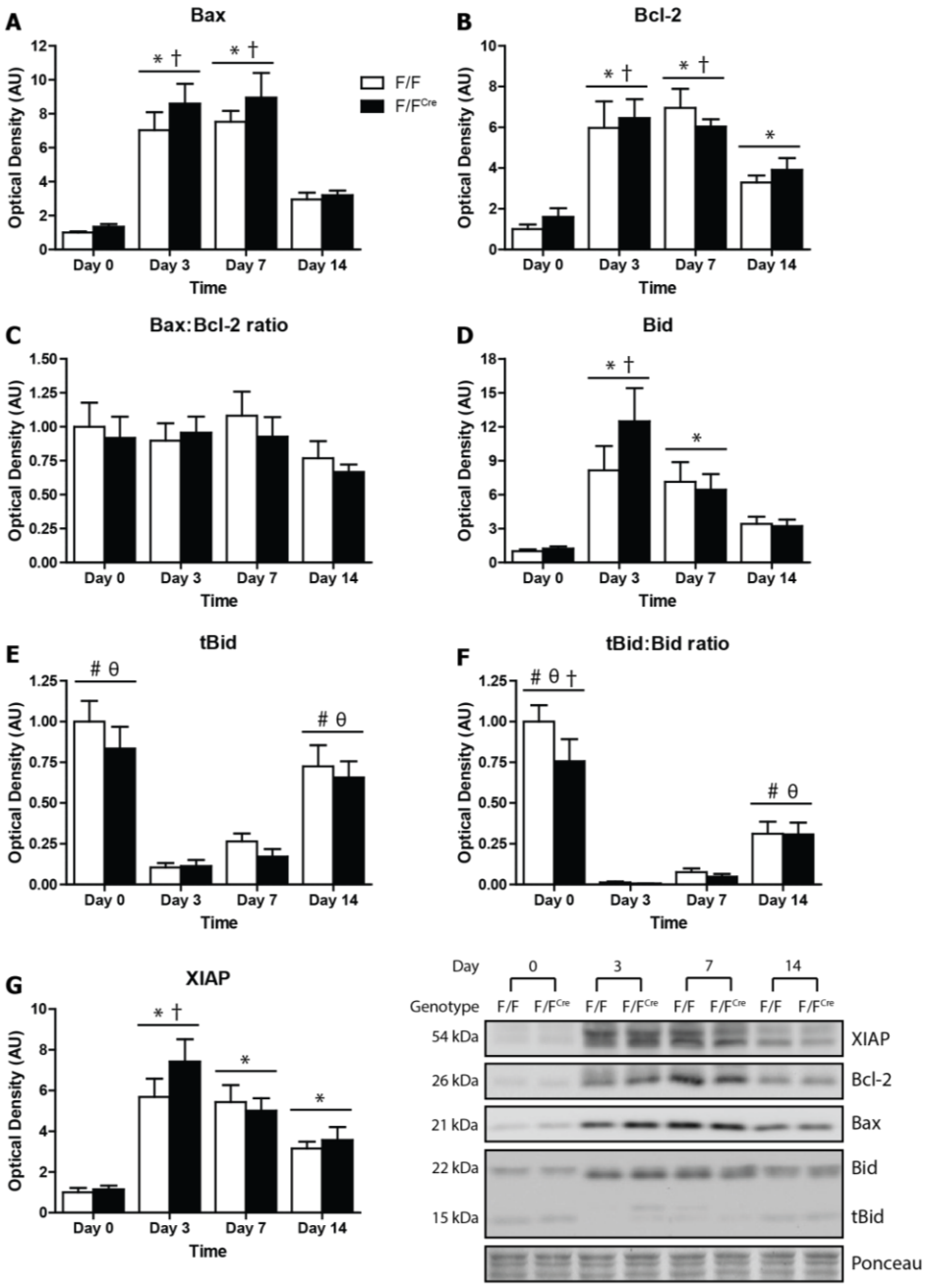

Figure 11: Apoptotic protein expression over the 14 day study period. Quantitative analysis of Bax (A), Bcl-2 (B), Bax:Bcl-2 ratio (C), Bid (D), tBid (E), tBid:Bid ratio (F), and XIAP (G) in the gastrocnemius (n=8 per group), along with representative immunoblots of each protein. * significant difference compared to day 0 (main effect). # significant difference compared to day 3 (main effect). θ significant difference compared to day 7 (main effect). † significant difference compared to day 14 (main effect).

Caspase and calpain activity in gastrocnemius after cardiotoxin injection

A significant main effect of time ($p<0.05$) was observed for caspase-3, with higher activity seen on day 7 compared to all other days, and on day 3 and 14 relative to day 0 (Figure 12A). Additionally, a main effect of time ($p<0.05$) was observed for caspase-8, which showed higher activity on day 7 relative to all other time points, and on day 14 compared to day 0 and 3 (Figure 12B). Caspase-9 also showed a main effect of time ($p<0.05$), with post hoc tests revealing higher activity again on day 7 compared to all other days, and on day 3 and 14 relative to day 0 (Figure 12C).

Calpain activity showed a significant effect of time ($p<0.05$) and also a trend ($p=0.10$) towards an interaction effect (Figure 12D). In reference to the time effect, calpain activity was elevated ($p<0.05$) on day 7 and day 14 relative to both day 0 and 3.

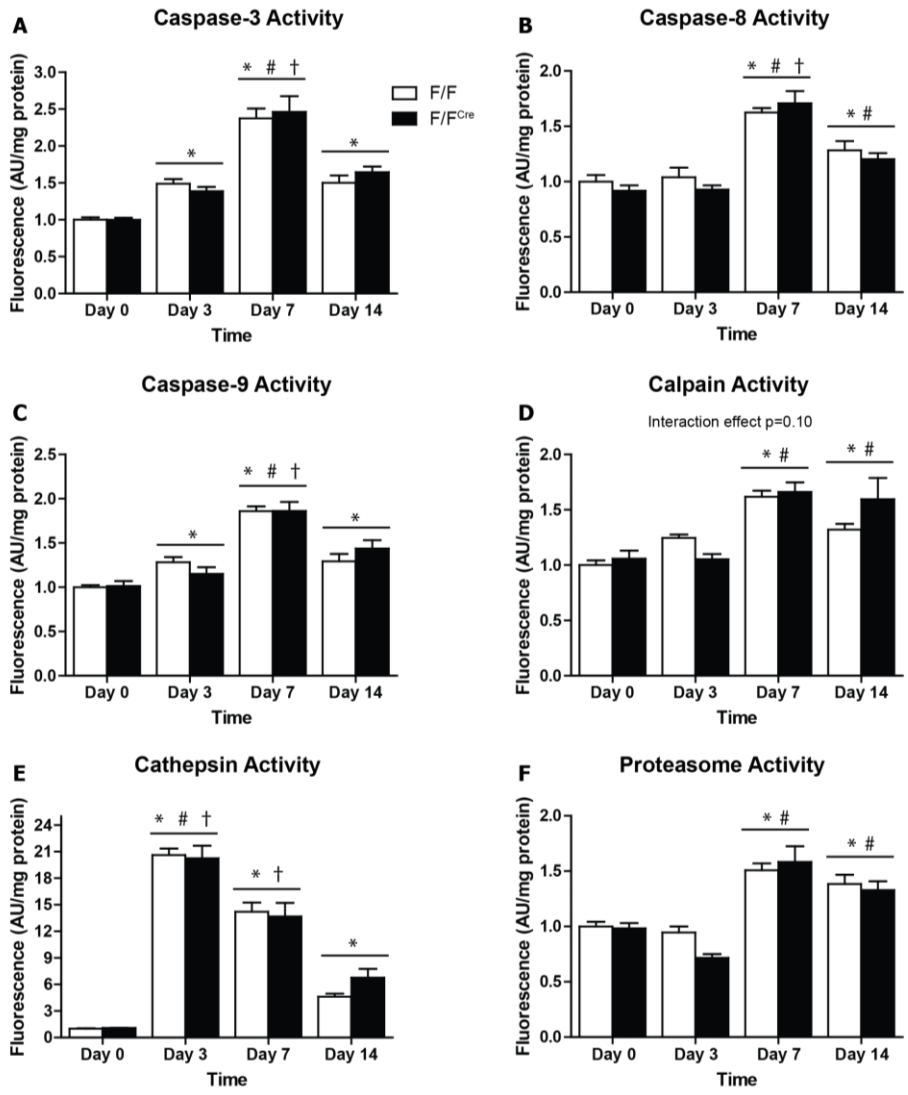

Figure 12: Enzyme activity over the course of the 14 day study period. Quantitative analysis of caspase-3 (A), caspase-8 (B), caspase-9 (C), calpain (D), cathepsin (E), and proteasome (F) activity in the gastrocnemius (n=8 per group). Statistical trend towards interaction effect is listed above graph if present. * significant difference compared to day 0 (main effect). # significant difference compared to day 3 (main effect). θ significant difference compared to day 7 (main effect). † significant difference compared to day 14 (main effect).

Expression of stress-related, antioxidant, and mitochondrial proteins, and ROS generation in gastrocnemius after cardiotoxin injection

A significant main effect of time ($p<0.05$) was seen for both Hsp70 (Figure 13A) and catalase (Figure 13B), with post hoc tests showing increased expression on day 3 and 7 relative

to day 0 and 14, and on day 14 relative to day 0. MnSOD levels also showed a main effect of time ($p<0.05$), with higher expression on day 0 compared to all time points, on day 14 compared to day 3 and 7, and on day 7 compared to day 3 (Figure 13C). Additionally, CuZnSOD showed a main effect of time ($p<0.05$), with day 0, 7, and 14 all showing higher ($p<0.05$) expression than day 3 (Figure 13D). A strong trend ($p=0.05$) towards increased CuZnSOD expression on day 0 relative to day 7 was also observed (statistical trend not noted on graph). Finally, a main effect of time ($p<0.05$) was observed for cytochrome c content, with day 0 showing significantly higher levels than day 3 (Figure 13E) and a trend ($p=0.06$) towards higher levels than day 7 (statistical trend not noted on graph). Elevated ($p<0.05$) cytochrome c expression was also seen on day 14 compared to day 3 and 7 (Figure 13E).

In regard to ROS production, a main effect of time ($p<0.05$) was discovered, with post hoc tests revealing increased ROS on day 3 and 7 compared to day 0, and on day 3 compared to day 14 (Figure 13F). A trend ($p=0.09$) towards higher ROS production on day 7 relative to day 14 was also observed (Figure 13F).

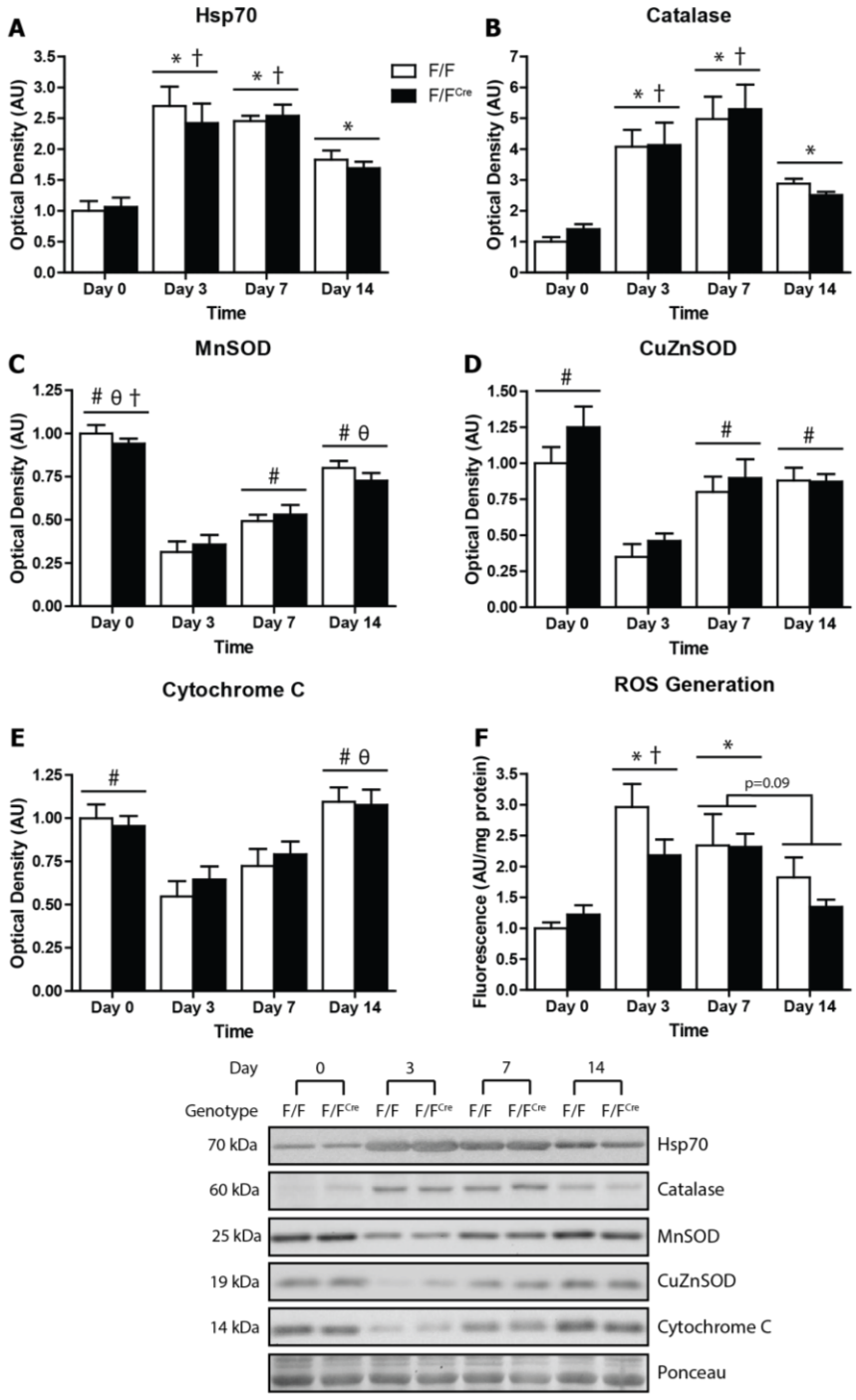

Figure 13: Expression of stress-related, antioxidant, and mitochondrial proteins, and ROS generation over the study period. Quantitative analysis of Hsp70 (A), catalase (B), MnSOD (C), CuZnSOD (D), and cytochrome C (E), as well as ROS generation (F) in the gastrocnemius (n=8 per group). Representative immunoblots of each protein are also presented. * significant difference compared to day 0 (main effect). # significant difference compared to day 3 (main effect). θ significant difference compared to day 7 (main effect). † significant difference compared to day 14 (main effect).

Muscle damage

No significant effects were observed when analyzing the proportion of damaged area on TA muscle cross-sections using a 2-way ANOVA, although there was a trend (p=0.07) towards a significant interaction effect (Figure 14A).

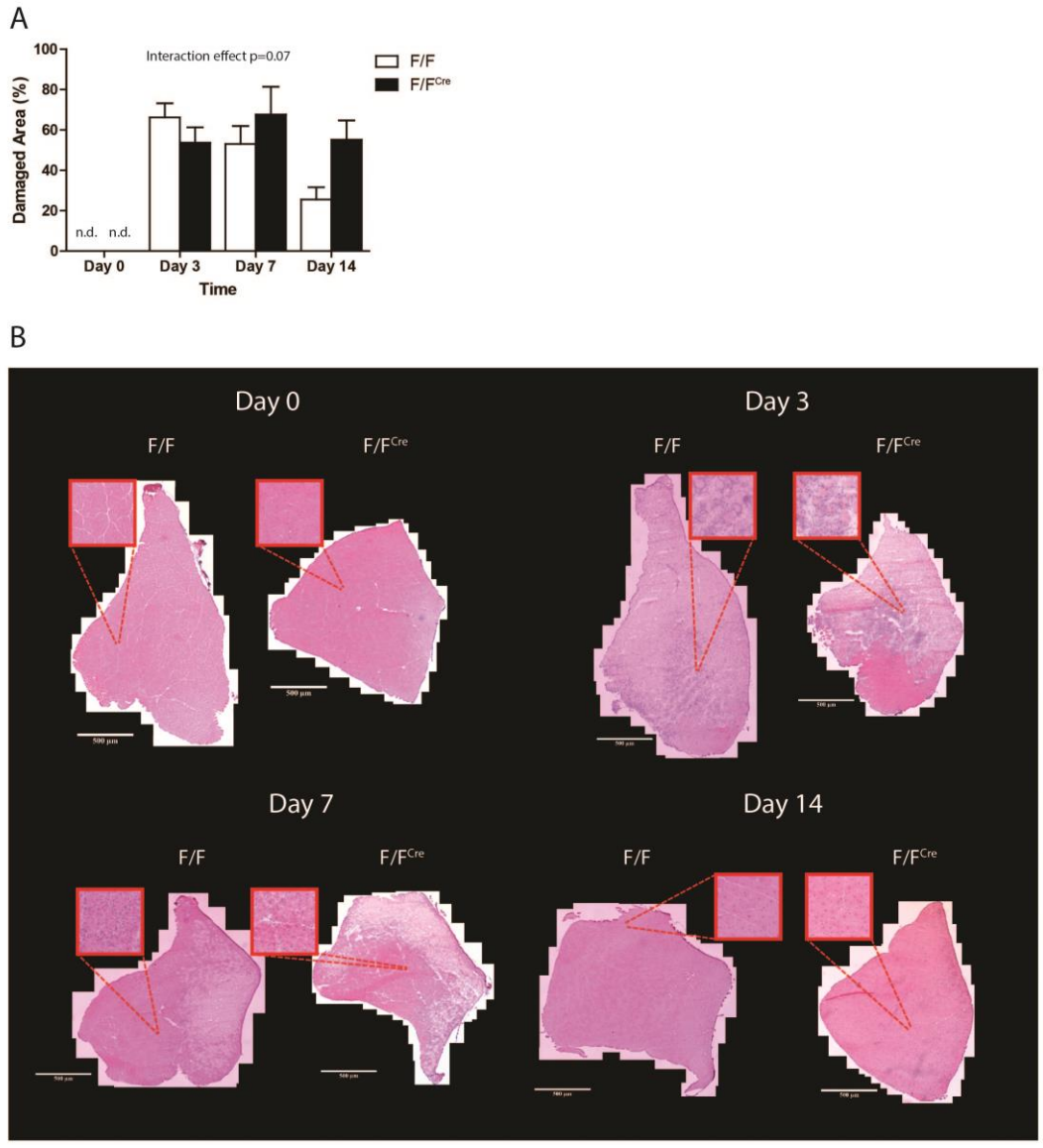

Figure 14: Muscle damage in TA after cardiotoxin exposure. Quantitative analysis of the damaged area in the muscle cross-sections as a percentage of the total area on day 3, 7, and 14 (A) (n=7 per group). No quantifiable damage was observed on day 0 in either group, therefore, a measure of damaged area was not determined (n.d.) at this time point. Also displayed are representative tibialis anterior cross-sections stained with H & E showing the progression of damage in both genotypes on day 0, 3, 7, and 14 (B). Interaction effect is listed above graph if present.

Tibialis anterior fiber type distribution, fiber type-specific CSA, and whole muscle CSA

A main effect of time ($p<0.05$) was observed for the percentage of type IIA fibers, with a higher percentage being seen on day 0 compared to day 14 (Figure 15A). In regards to type IIA/X fibers, a main effect of time ($p<0.05$) and a main effect of genotype ($p<0.05$) were discovered, with the percentage of type IIA/X fibers being higher on day 14 relative to day 0, and in the F/F^{Cre} animals compared to the F/F animals (Figure 15B). No effects were observed in the distribution of type IIX fibers (Figure 15C). Conversely, a main effect of time ($p<0.05$) was seen when examining the percentage of type IIX/B fibers, with a higher percentage on day 14 relative to day 0 (Figure 15D). Finally, a main effect of time ($p<0.05$) was observed for the percentage of type IIB fibers, with a higher percentage being seen on day 0 relative to day 14 (Figure 15E). A trend ($p=0.07$) towards a main effect of genotype was also observed for the percentage of type IIB fibers (Figure 15E). Of note, a significant main effect of time ($p<0.05$) was observed when examining the total number of fibers in the muscle cross-sections, with a higher number of fibers being seen on day 14 compared to day 0 (Figure 15F).

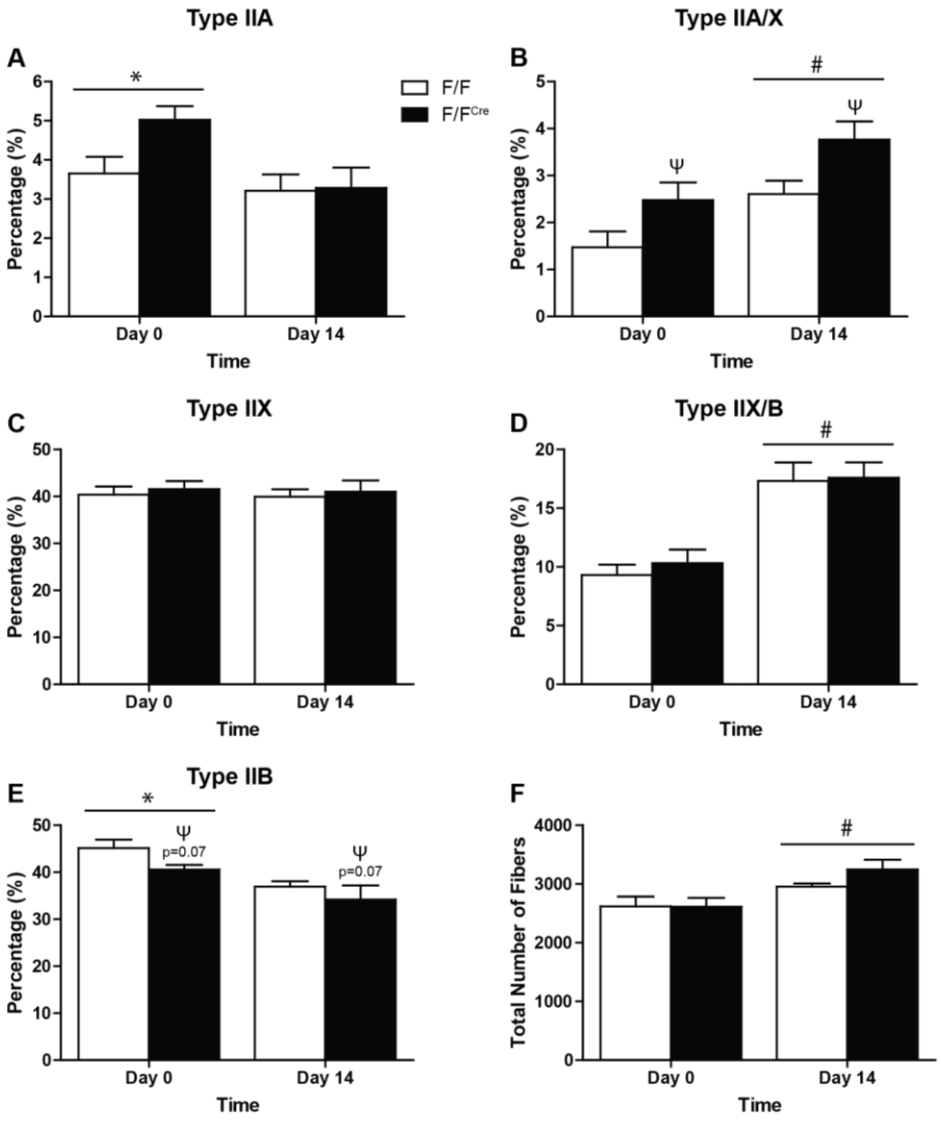

Figure 15: Muscle fiber type distribution and total fiber number in tibialis anterior. Quantification of the percentage of type IIA (A), IIA/X (B), IIX (C), IIX/B (D), and IIB (E) fibers in the muscle cross-sections. Quantification of total fiber number (F) is also presented (n=6 per group). * significant difference compared to day 14 (main effect). # significant difference compared to day 0 (main effect). Ψ significant difference compared to F/F (main effect).

Analysis of fiber type cross-sectional area in the TA revealed a significant interaction effect ($p<0.05$) for type IIA (Figure 16A), IIX (Figure 16C), and IIX/B fiber CSA (Figure 16D). Post hoc analysis revealed increased type IIA and IIX fiber CSA in the F/F^{Cre} mice on day 14 compared to the F/F^{Cre} mice on day 0, and compared to the F/F mice on day 0 and 14 (Figure

16A and Figure 16C). Additionally, post hoc tests displayed increased type IIX/B fiber CSA in the F/F^{Cre} animals on day 14 relative to the F/F^{Cre} animals on day 0, and relative to the F/F animals on day 14 (Figure 16D). A significant interaction effect ($p<0.05$) was also seen for type IIB fiber CSA (Figure 16E), although post hoc tests did not reveal any significant differences. For type IIA/X fibers (Figure 16B), a trend ($p=0.06$) towards a significant interaction effect was discovered, as was a significant main effect of genotype ($p<0.05$), with the F/F^{Cre} group displaying higher average type IIA/X fiber CSA compared to the F/F group. A trend ($p=0.05$) towards a significant main effect of time was also observed for type IIA/X fiber CSA. A significant interaction effect ($p<0.05$) was observed when analyzing whole muscle cross-sectional area of the TA (Figure 16F). Post hoc analysis displayed no CSA differences between day 0 and 14 in the F/F mice, while a trend ($p=0.07$) towards a significant increase in CSA was seen over this time in the F/F^{Cre} mice.

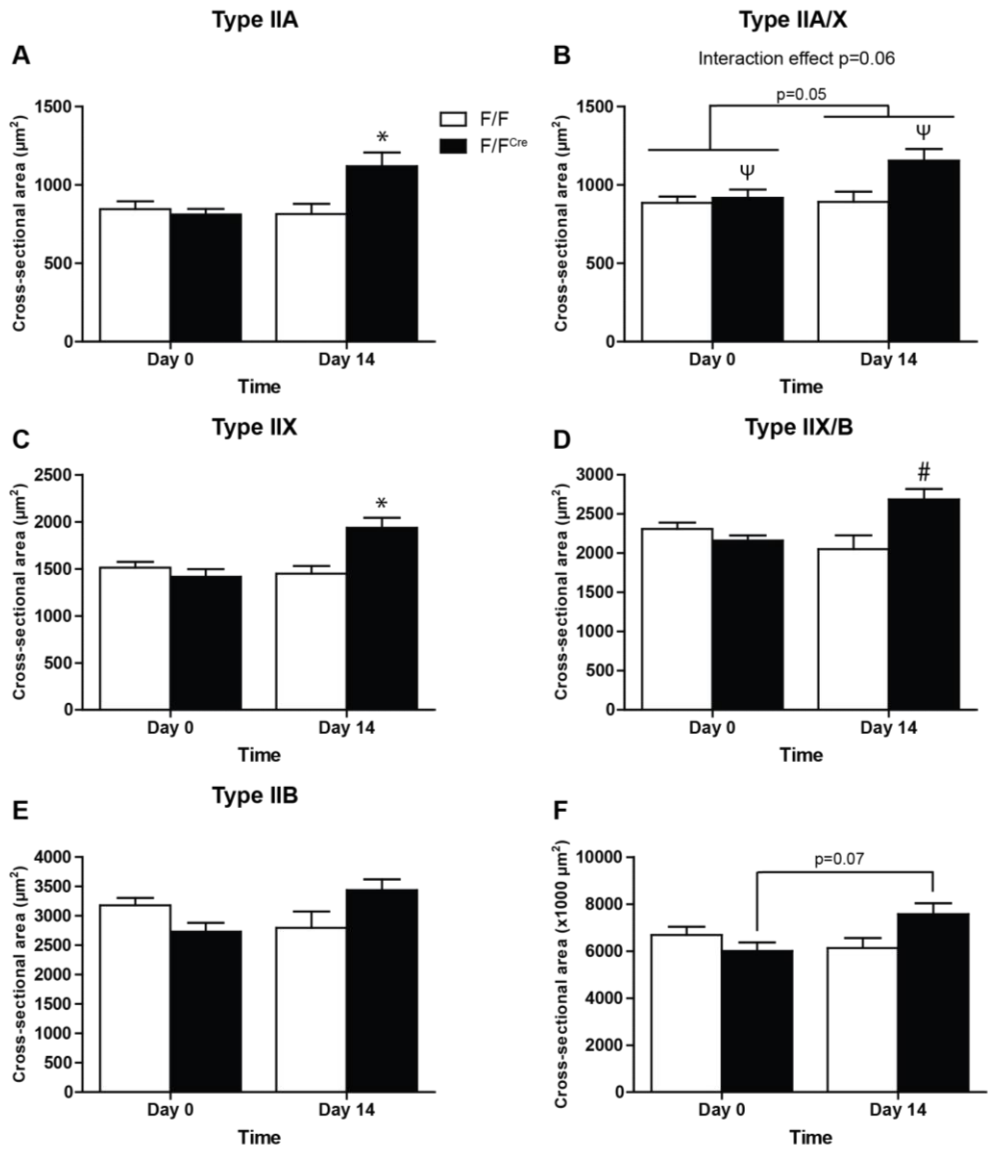

Figure 16: Fiber type cross-sectional area and whole muscle cross-sectional area in TA. Quantification of type IIA (A), IIA/X (B), IIX (C), IIX/B (D), and IIB (E) fiber cross-sectional area, as well as whole muscle cross-sectional area (F) (n=6 per group). Statistical trend towards interaction effect is listed above graph if present. * significant difference compared to all other bars (interaction effect). # significant difference compared to F/F^{Cre} day 0 and F/F day 14 (interaction effect). Ψ significant difference compared to F/F (main effect).

Discussion

The goals of this Master's thesis were to investigate the role of autophagy in modulating apoptotic signaling in skeletal muscle following cardiotoxin-induced muscle injury, and to examine the role that autophagy plays in skeletal muscle recovery after cardiotoxin-induced muscle damage. It was believed that using a skeletal muscle-specific Atg7 knockdown (i.e. autophagy deficient) mouse model would be an ideal way to answer these questions. Furthermore, it was believed that using a tamoxifen inducible knockdown model rather than a constitutive knockdown model would provide more applicable conclusions as the inducible knockdown mice maintain their autophagic capabilities during development and up until the point of tamoxifen injection, whereas gene recombination and autophagy inhibition occur throughout the life cycle in the constitutive knockdown mice[71]. Therefore, the inducible knockdown model was thought to be more appropriate to study because these mice circumvent any potential adaptations that may have occurred during development in the constitutive knockdown mice to compensate for the lack of autophagy. Tamoxifen-inducible, skeletal muscle-specific Atg7 knockdown mice have been studied previously in the literature to examine the role of autophagy under basal conditions, during exercise, and during aging (this will be discussed in more detail below)[72-74]. However, these animals have not been used to investigate the role of autophagy in conditions of acute, extensive muscle trauma like those imposed in this Master's thesis.

In 2009, Masiero and colleagues examined constitutive skeletal muscle-specific Atg7 knockout (KO) mice as well as tamoxifen-inducible, skeletal muscle-specific Atg7 KO mice similar to the one used in the current Master's thesis[72]. Under basal conditions, ATG7 protein expression was nearly undetectable in 2 month old constitutive Atg7 KO mice, and the small amounts discovered by immunoblots were attributed to the presence of other cells (e.g. fibroblasts, blood cells, etc.) within the muscle[72]. This extensive Atg7 KO led to an accumulation of p62 and to an inhibition of LC3-I lipidation in both oxidative and glycolytic muscles. The inhibition of autophagy in these constitutive Atg7 KO animals caused degenerative changes such as increased vacuolated and centrally nucleated fibers, as well as atrophy of oxidative and glycolytic fibers (in both males and females)[72]. Additionally, these authors found increased MAFbx and MuRF1 expression, increased proteasome activity, and increased apoptotic nuclei in these mice[72]. Electron microscopy also revealed a misalignment of z-discs, sarcoplasmic reticulum distension, and an accumulation of swollen, abnormal mitochondria, and in the constitutive Atg7 KO mice[72]. Moreover, the observed mitochondrial dysfunction lead to increased oxidative stress as seen by elevated levels of protein carbonylation[72]. Finally, a decrease in both absolute and specific muscle force was discovered in the constitutive Atg7 KO animals[72]. While the analysis was not quite as extensive, these authors found a similar expression profile for ATG7, p62, and LC3, similar morphological alterations and atrophy, and similar decreases in muscle force in the tamoxifen-inducible, skeletal muscle-specific Atg7 KO mice compared to the constitutive KO animals[72]. Interestingly, more centrally nucleated fibers were seen in the inducible KO mice relative to the constitutive KO mice[72]. In the current Master's thesis, a significant decrease (~61%) in ATG7 expression was observed in the gastrocnemius of the F/F^{Cre} animals on day 0, however this decrease was not as drastic as that seen by Masiero and

colleagues. This less extensive Atg7 knockdown likely accounts for the lack of p62 accumulation and for the relatively decreased inhibition of LC3 lipidation in the F/F^{Cre} animals on day 0 relative to the mice examined in the Masiero study. Furthermore, these differences in ATG7, p62, and LC3 expression suggest a reduced inhibition of autophagy in the current thesis compared to that achieved by Masiero et al., which could explain the different results obtained between the two studies. It is possible that a lower degree of autophagy inhibition in the current thesis was accompanied by a reduced accumulation of cellular debris (as seen by an absence of p62 accumulation) and damaged mitochondria, resulting in similar levels of ROS production and fiber regeneration (i.e. as seen by a lack of an increase in centrally nucleated fibers) between the F/F and F/F^{Cre} animals on day 0. Decreased autophagy inhibition may also explain why fiber atrophy was limited to glycolytic fibers in the current thesis. Previous research has suggested a decreased reliance on autophagy in oxidative fibers, as evidenced by much lower levels of autophagic flux in oxidative muscle (soleus) compared to glycolytic muscle (extensor digitorum longus) in colchicine-treated, wild-type mice under basal conditions (unpublished work, Quadrilatero lab). The idea of increased reliance on autophagy in glycolytic fibers is also supported by a study by Mizushima and colleagues, who found a faster and greater activation of autophagy in glycolytic muscle (EDL) compared to oxidative muscle (soleus) in response to fasting by examining levels of LC3 protein tagged with green fluorescent protein (GFP)[75]. Another study by Ogata and colleagues also demonstrated greater autophagic activation in glycolytic muscle (plantaris) compared to oxidative muscle (soleus) in response to fasting as seen by faster and greater increases in LC3B-II and p62 in the plantaris[76]. Consequently, in contrast to the study by Masiero and colleagues, it is possible that the level of autophagy inhibition achieved in this Master's thesis was not great enough to cause atrophy in the more

oxidative fiber types. Finally, the decreased inhibition of autophagy in the current study probably explains the lack of a compensatory increase in UPS system activity like that seen by Masiero and colleagues. Clearly, a difference between the knockout models used by Masiero et al. and the current thesis exists, which led to dramatic variations in the results obtained under basal conditions.

Other studies examining the effects of autophagy inhibition under basal conditions in constitutive, skeletal muscle-specific Atg7 KO mice have also found reductions in ATG7 protein in conjunction with an accumulation of p62 and decreased LC3 lipidation[77, 78]. In agreement with the current study, Kim et al. discovered lower body and gastrocnemius weight as a result of muscle-specific autophagy inhibition[77]. Interestingly, while predominantly glycolytic muscles (i.e. TA, gastrocnemius, plantaris) underwent atrophy in the F/F^{Cre} mice on day 0, atrophy of the more oxidative soleus muscle was not observed under basal conditions. This could suggest that oxidative muscles are less susceptible to autophagy inhibition-induced muscle atrophy, possibly due to the decreased reliance on autophagy in oxidative fibers as discussed above. Also similar to the current thesis, Wu and colleagues found no apparent morphological abnormalities in the Atg7 KO mice compared to the control mice on H & E stained muscle cross-sections[78]. However, Wu et al. did discover an accumulation of abnormal, swollen mitochondria along with decreases in mitochondrial function in their Atg7 KO animals, and increased ROS production in murine embryonic fibroblasts (MEFs) isolated from Atg7 KO embryos[78]. While the current thesis did not examine mitochondrial morphology or function, no increases in ROS production were discovered in the F/F^{Cre} mice on day 0; however, it should be noted that the assay used in this study was a general measure of ROS rather than a mitochondrial-specific ROS measurement. It

is possible that constitutive muscle-specific Atg7 KO has a greater effect on the mitochondria, resulting in higher levels of ROS generation.

As mentioned above, tamoxifen-inducible, skeletal muscle-specific Atg7 knockdown mice similar to those used in the current Master's thesis have been used to investigate the role of autophagy during exercise[73]. This study by Lo Verso et al. (which used the same mice as the Masiero et al. study) found that under basal conditions, the Atg7 knockout animals displayed marked increases in p62 and LC3-I, and increased levels of mitochondrial dysfunction and ROS generation[73]. Again, no differences in basal ROS production were observed in the current thesis, perhaps due to a lower degree of autophagy inhibition. These authors also found that when subjected to concentric (uphill) treadmill exercise to exhaustion, neither male nor female Atg7 knockout mice showed differences in running capacity or morphological signs of damage compared to controls[73]. In contrast, when subjected to a single bout of eccentric (downhill) treadmill running, decreased running capacity was observed in the Atg7 knockout mice, but this effect was limited to the female animals[73]. Furthermore, after 3 days of eccentric exercise, female Atg7 knockout mice again displayed decreased running capacity relative to controls[73]. Notably, this decreased performance was not caused by any exercise-related structural alterations, as no signs of inflammation, necrosis, or plasma membrane disruption were seen in the muscles of the female Atg7 knockout or control animals[73]. The absence of major morphological alterations in these animals after eccentric exercise is noteworthy since this type of exercise is commonly thought to promote muscle damage. The sex-specific effect of autophagy inhibition on exercise performance is also notable and suggests that future research investigating autophagic mechanisms should examine both male and female subjects. Despite different in running capacity, both male and female Atg7 KO mice displayed a decrease in

mitochondrial function over time as a result of eccentric exercise, although the effect was greater in females[73]. This mitochondrial dysfunction was associated with increased ROS production; however, this did not seem to be the cause of decreased running capacity in the female Atg7 knockout animals as treatment with an antioxidant did not improve their running performance[73] . Overall, the authors concluded that autophagy plays a major role in maintaining mitochondrial function during exercise[73]. As previously discussed, the current thesis did not conduct any direct measures of mitochondrial function, but it would be interesting to see how the mitochondria responded to cardiotoxin-induced damage in mice that remained autophagy deficient throughout the process of muscle recovery. Since autophagy normally plays a role in cell quality control and removing damaged mitochondria, it is hypothesized that an inhibition of autophagy during cardiotoxin exposure would lead to an accumulation of dysfunctional mitochondria, which could subsequently lead to delayed muscle regeneration due to deficient energy production in the cell.

Finally, a study by Carnio and colleagues investigated the role of autophagy at the neuromuscular junction (NMJ) and during aging using the same inducible Atg7 KO mice as the Masiero et al study[72, 74]. These authors induced a skeletal muscle-specific inhibition of autophagy in 22 month old mice, which they sacrificed 3 months later. They found that suppressing autophagy led to an accumulation of p62 and LC3-I, as well as increased levels of muscle breakdown as evidenced by an approximately 2-fold increase in centrally nucleated fibers and by a decrease in fiber cross-sectional area[74]. Another observation in this study was that the Atg7 knockout mice displayed an increase in neural cell adhesion molecule (NCAM)-positive cells compared to aged matched controls, suggesting a significant loss of muscle innervation since NCAM becomes highly expressed along the entire length of adult muscle fibers if denervation occurs[74]. It should be noted that while these authors showed an accumulation of p62 and LC3-I

in the 25 month old Atg7 KO mice (i.e. 3 months after autophagy inhibition), they did not measure ATG7 expression (or at least did not present a measurement of ATG7) in these animals. It is possible that some ATG7 restoration could have occurred in these animals since some level of muscle regeneration and satellite cell incorporation may have taken place over the 3 month intervention period. On the other hand, perhaps the amount of muscle regeneration taking place in these mice was so low that there was no significant satellite cell activation, and in turn, there was no significant ATG7 restoration. Whatever the case, future studies using inducible, skeletal muscle-specific Atg7 knockdown mice should examine ATG7 protein content after the intervention period to confirm that the knock down of Atg7 is maintained. An additional interesting finding of this study was that autophagy was shown to decrease with age in both mice and humans[74]. The authors questioned whether this reduction in autophagy may play a role in the muscle degeneration seen with aging, so they overexpressed ATG7 in aged (26 month old) F/F mice to see if restoring autophagic flux helped to reduce muscle breakdown. Indeed, it was discovered that the mice overexpressing ATG7 displayed decreased fragmentation of the NMJ, a reduced number of NCAM-positive fibers, and increased muscle mass compared to age-matched controls[74]. These results suggest that autophagy inhibition during aging is involved with muscle atrophy, and that the enhancement of autophagic signaling in skeletal muscle during aging could play a role in preventing sarcopenia. Results from the current thesis also showed that restoring autophagic function could promote enhancements in muscle mass, as muscle weights returned to control levels in the F/F^{Cre} mice on day 14 (i.e. when ATG7 expression was restored in these animals)(Appendix Figure A2) despite weighing less on day 0 (i.e. when ATG7 expression was reduced). Interestingly, autophagy inhibition-induced muscle atrophy seemed to be limited to glycolytic muscles in the current thesis, as TA, gastrocnemius, and plantaris muscle weights

were reduced in the F/F^{Cre} mice compared to the F/F mice on day 0, but soleus weight was not different between groups at this time point. This could be due to a greater reliance on autophagy in glycolytic muscles as discussed above.

Despite the promising potential conclusions that could have been derived from studying tamoxifen-inducible, skeletal muscle-specific Atg7 KO mice in this thesis, it appears as though this was not the best animal model to use in conjunction with an intervention causing widespread muscle damage and regeneration (e.g. cardiotoxin injury). While the model proved to cause a significant knockdown of the Atg7 gene and a significant corresponding reduction of ATG7 protein in a skeletal muscle-specific manner on day 0 (i.e. prior to cardiotoxin treatment), this did not remain true after intramuscular cardiotoxin injections. As seen above, ATG7 protein expression increased dramatically in the F/F^{Cre} animals 3 days after cardiotoxin injection. Beyond day 3, similar ATG7 protein expression was observed between groups, showing that both groups had a similar genetic composition on day 7 and 14. This was unfortunate as it was hoped that the Atg7 knockdown would persist throughout the 14 day study period to allow for examination of the apoptotic response to muscle injury and of the skeletal muscle recovery process in absence of autophagy in the F/F^{Cre} animals. It was interesting to see that the Atg7 knockdown did persist in the undamaged quadriceps muscle on day 14, as this verified the fact that the return of ATG7 protein expression was associated with the induction of damage and was not simply caused by a problem with the functionality of the model. Additionally, this information provided clues as to why the expression of Atg7 was restored in the F/F^{Cre} mice post-cardiotoxin injection.

In the mouse model used for this study, Cre-driven recombination of the Atg7 gene was under control of the HSA promoter. The α-skeletal actin protein isoform produced by this gene is

highly expressed in skeletal muscle[79], and in turn, large amounts of the MerCreMer protein complex would also be expressed. Conversely, quiescent satellite cells do not express α-skeletal actin[80], and in turn would not express the MerCreMer protein complex. Additionally, it is important to note that quiescent satellite cells are located between the sarcolemma and the basal lamina of the muscle fibers, and therefore are not part of the muscle fibers themselves[81]. These facts can be used to see that the tamoxifen injections caused Atg7 knockdown in the myonuclei but not in the quiescent satellite cell nuclei. Due to the high expression levels of the MerCreMer protein complex in the muscle (i.e. because of high HSA promoter activity), tamoxifen injection would cause this complex to translocate from the cytoplasm into the myonuclei and cause recombination of the Atg7 gene. Alternatively, the quiescent satellite cells did not express the MerCreMer complex in their cytoplasm, and in turn, no recombination of the Atg7 gene occurred in the satellite cell nuclei despite the injection of tamoxifen. Moreover, since the quiescent satellite cells are separate from the muscle fibers, the MerCreMer complexes present in the muscle would not be able to gain access to the satellite cell nuclei even in the presence of tamoxifen. Consequently, as the muscle recruited satellite cells in order to regenerate after the cardiotoxin-induced damage, it regained nuclei that possessed the Atg7 gene. This led to a subsequent increase in ATG7 protein and an elimination of the Atg7 knockdown. Importantly, the knockdown of the Atg7 gene and the reduction of ATG7 protein were not restored after satellite cell fusion because tamoxifen was no longer in the animals' system since injections of tamoxifen were no longer being administered. Accordingly, even though more of the MerCreMer protein complex was being produced through activation of the HSA promoter during muscle cell differentiation and remodeling, it was not able to translocate to the nucleus and cause Atg7 recombination.

The literature regarding satellite cells has found that satellite cell activation, proliferation, and fusion begins 1-2 days after muscle injury[82]. Satellite cell activation is thought to be promoted by a variety of signals. These signals include the production of sphingosine-1-phosphate inside the plasma membrane of the satellite cell[83], and a nitric oxide-dependent release of hepatocyte growth factor (HGF), which binds to receptors on the satellite cells[84]. While HGF appears to activate and promote proliferation of satellite cells, it also seems to inhibit differentiation of these cells[85]. The transition from satellite cell proliferation to differentiation is thought to depend on the balance between Notch and Wnt signaling, as Notch signaling is elevated early on after muscle injury as the satellite cells proliferate, while Wnt signaling increases significantly as early as 2 days after muscle injury and continues to increase over time as the satellite cells differentiate[86]. On a related note, a study by Sesodia and colleagues showed that some enzymes can regain normal activity levels as early as 3 days after muscle damage induced by notexin (i.e. a myotoxin derived from tiger snake venom)[87]. These findings help to further explain how ATG7 protein levels were restored as early as day 3 in the F/F^{Cre} animals in the current study. Within the first couple of days after cardiotoxin-damage, satellite cells in the injured muscle were activated and proliferated. Then, as early as 2 days after injury, these satellite cells differentiated and matured into functional myonuclei. At this point, these new myonuclei began to transcribe mRNA which was subsequently translated into protein. Since autophagy appears to be upregulated in response to muscle damage (i.e. as evidenced by increased ATG7 and Beclin-1 protein content, as well as cathepsin activity in the F/F mice), and these new myonuclei contained copies of the Atg7 gene in their DNA, an increase in ATG7 protein occurred in the F/F^{Cre} animals.

Another factor that may have contributed to the increased ATG7 expression in the F/F^{Cre} mice after cardiotoxin injection is the possibility that gene recombination did not occur in all of the myonuclei. As discussed above, previous research in Atg7 KO animals has shown extensive ATG7 knockdown and subsequent increases in p62 and LC3-I content[72, 73, 78]. Conversely, ATG7 expression was only decreased by ~61% in the gastrocnemius of the F/F^{Cre} mice in the current thesis, and no significant accumulation of p62 or LC3B-I was observed on day 0. The less extensive knockdown of Atg7 and less severe inhibition of autophagy in the F/F^{Cre} mice may signify that some myonuclei maintained the ability to generate ATG7 protein even after tamoxifen administration. If true, these $Atg7^{+/+}$ myonuclei could have upregulated ATG7 production in response to cardiotoxin exposure, contributing to the observed restoration of ATG7 content. Additionally, the infiltration of various cell types such as macrophages, neutrophils, and blood cells into the muscle after cardiotoxin injury could have contributed to the increased ATG7 expression measured by immunoblotting since these cells would have also been present in the muscle homogenates that were analyzed.

Although definitive conclusions regarding the effects of autophagy inhibition on apoptotic signaling and muscle regeneration could not really be drawn due to the restoration of ATG7 content in the F/F^{Cre} animals, it was still possible to evaluate the autophagic and apoptotic responses to cardiotoxin-induced muscle injury and the relationship between the two pathways. Marked increases in ATG7, LC3B-II, Beclin-1, ATG4B, and cathepsin activity along with a drastic decrease in p62 content were observed on day 3, suggesting a large upregulation of autophagic flux at this time point. This increased autophagic signaling likely occurred in order to remove the large amounts of damage produced by cardiotoxin exposure. Furthermore, autophagic flux appeared to remain significantly elevated on day 7, as ATG7 and ATG4B

content remained increased and the expression of LC3B-I, LC3B-II, and Beclin-1 increased to levels greater than those seen on day 3. Notably, p62 expression increased slightly and cathepsin activity was slightly reduced on day 7 compared to day 3. These findings seem to indicate that autophagic flux peaked on day 3 and began to decrease slightly on day 7, as a rise in p62 content suggests a decrease in autophagy (i.e. since p62 is normally degraded by autophagy)[72] and decreased cathepsin activity suggests a reduction in autophagosome breakdown (i.e. since cathepsins are lysosomal enzymes that contribute to autophagosome degradation)[88]. On day 14, ATG7, ATG4B, LC3B-I, and Beclin-1 content was reduced compared to day 7, as was cathepsin activity. Additionally, the expression of p62 returned to the basal levels seen on day 0, suggesting a further decrease in autophagic flux relative to day 7. Interestingly, LC3B-II content and the LC3B-II:I ratio remained elevated to the same level as seen on day 7. Overall, the results obtained in the current study indicate that autophagic flux was stimulated by cardiotoxin-induced damage, peaked on day 3, and then continued to decrease over time. Notably, it is possible that autophagic flux actually peaked somewhere between day 3 and day 7; however, this could not be determined since no time points were analyzed between these two days. It was interesting to see that the UPS system seemed to respond in an opposite manner compared to autophagy after cardiotoxin-induced damage. Expression of both MAFbx and MuRF1 was significantly reduced on day 3 and 7 relative to day 0, but was increased on day 14 compared to day 3 and 7. It was also observed that proteasome activity did not increase compared to day 0 until day 7, and this activity remained elevated on day 14. This is noteworthy since increases in both autophagy and UPS activation have been observed under atrophic conditions[72, 89]. It appears that the coordination of these two degradative pathways is different in response to acute muscle damage as compared to more chronic atrophy conditions, and that increased activity of one of these

proteolytic systems can result in decreased activity of the other system. Indeed, an upregulation of autophagy along with decreased activity of the UPS has been seen before and vice versa[72, 90].

Interestingly, apoptotic signaling showed a different activation profile compared to autophagic signaling. While caspase-3 and caspase-9 activity was slightly increased on day 3 compared to day 0, the activity of these enzymes, along with caspase-8 and calpains, did not peak until day 7. The activity of these enzymes then decreased on day 14 (with the exception of calpains), but remained elevated compared to day 0. Notably, while Bax expression increased on day 3 and day 7, so too did Bcl-2 expression causing a similar Bax:Bcl-2 ratio between days. This increase in anti-apoptotic Bcl-2 along with increases in the anti-apoptotic protein XIAP on day 3 and 7 likely represented a cellular response to suppress extreme elevations in apoptotic signaling. Increases in Hsp70 and catalase content on day 3 and 7 may have also represented an attempt to inhibit elevations in apoptotic signaling and suppress increases in ROS production.

Overall, these findings regarding autophagic and apoptotic signaling suggest that autophagy is activated to a greater degree early on after cardiotoxin injury, while the activation of apoptosis occurs slightly later. From these results, it is hypothesized that autophagy is more involved in the response to muscle damage and in the "cleanup" of the muscle fibers after acute injury, while apoptosis is more involved in the remodeling and regeneration of muscle fibers. This is speculated because the inflammatory response to cardiotoxin-induced damage has been shown to peak 1-4 days after cardiotoxin injection, while the regeneration of muscle fibers has been observed to occur ~5-6 days after cardiotoxin treatment[91]. These results also suggest that although autophagy activation is followed by increased apoptotic signaling in response to skeletal muscle damage, this level of apoptosis is not necessarily associated with an induction of cell death as the muscle fibers actually regenerate rather than die. In fact, the activation of

autophagy may represent a cellular response that indirectly suppresses apoptotic signaling and prevents higher levels of cell stress and atrophy. Indeed, decreased expression of cytochrome c, MnSOD, and CuZnSOD was observed on day 3, the same time that autophagic signaling appeared to peak. Reductions in cytochrome c and MnSOD may represent an induction of mitophagy (i.e. autophagic breakdown of mitochondria) in order to eliminate dysfunctional mitochondria that would otherwise produce high levels of superoxide which could elevate apoptotic signaling. Decreased CuZnSOD expression on day 3 supports this idea as this enzyme normally helps to degrade superoxide in the cytosol and prevent oxidative stress[92]. Furthermore, extreme reductions in tBid expression and the tBid:Bid ratio were observed on day 3 and day 7 when autophagic signaling was elevated. Activated tBid has been shown to facilitate cytochrome c release from the mitochondria and consequently cause an activation of caspases[93]. Therefore, large reductions in tBid, potentially as a result of autophagy-mediated degradation (i.e. since autophagic activity was greatly increased on day 3 and 7 at the time of tBid degradation), may represent another mechanism of apoptosis inhibition by autophagy.

All in all, while some research has associated concomitant elevations of autophagic and apoptotic signaling with toxic effects[94-96], and consequently it has been proposed that autophagy is a cytotoxic process, the current thesis suggests that this may not be the case. Early increases in autophagy after cardiotoxin injury were met by only slightly elevated levels of apoptotic signaling, and apoptotic activity did not appear to peak until autophagic signaling had begun to decrease. These results demonstrate that examining the timing of the increased autophagic and apoptotic signaling by analyzing different time points is equally important as investigating the absolute elevations in signaling. When this approach was taken in the current Master's thesis, it appeared that autophagy induction may have played a cytoprotective role in skeletal muscle after

cardiotoxin exposure by potentially reducing cell stress and indirectly blunting the apoptotic response. It would have been very interesting to see if apoptotic signaling was elevated earlier and/or to a greater extent in the F/F^{Cre} mice had the knockdown of Atg7 persisted, as this would have more definitely elucidated whether autophagic activation was involved in suppressing apoptotic signaling. Indeed, a study by McMillan & Quadrilatero showed that an inhibition of autophagy by 3-methyladenine (3MA) during myoblast differentiation caused increased transient caspase-3 activation, apoptotic nuclei, and DNA fragmentation[97]. An inhibition of autophagy by Atg7 shRNA also caused elevated DNA fragmentation in differentiating myoblasts[97]. Additionally, this study showed that autophagic signaling increased transiently during myoblast differentiation[97]. This suggests that the differentiation of satellite cells in the regenerating muscle could have contributed to the early increases in autophagy seen in the current thesis. The differentiation of satellite cells could have also contributed to the observed increases in apoptotic signaling after cardiotoxin exposure, as myoblast differentiation has been shown to cause transient increases in caspase-3 activity[98]. Future studies examining autophagic and apoptotic signaling should play close attention to the temporal relationship between these two processes.

Further evidence of a cytoprotective role of autophagy after cardiotoxin injury can be speculated from the autophagic protein expression, calpain activity, and ROS generation data obtained in the current study. Although not found to be statistically significant by 2-way ANOVA, it appears as though ATG7, ATG4B, and LC3B-II content was slightly higher in the F/F^{Cre} mice on day 3 compared to the F/F mice. Increased expression of these proteins may suggest an elevation of autophagic induction in the F/F^{Cre} animals at this time point since ATG4 converts pro-LC3 to LC3-I, ATG7 helps to convert LC3B-I to LC3B-II, and increased LC3B-II is associated with an increased number of autophagosomes[35, 99]. This increased autophagic

activity on day 3 may have been a compensatory response in the F/F^{Cre} mice due to the fact that autophagy was initially inhibited in these animals. Additionally, although again not shown to be statistically significant, calpain activity and ROS generation seemed to be slightly reduced in the F/F^{Cre} group relative to the F/F group on day 3. These results could indicate that increased autophagic flux in the F/F^{Cre} animals on day 3 suppressed elevations in calpain activity and ROS generation.

It was interesting to see that despite a restoration of ATG7 protein in the F/F^{Cre} animals, the area occupied by damaged and centrally nucleated fibers in tibialis anterior cross-sections from these mice appeared to be elevated on day 14 post-cardiotoxin injury relative to the F/F mice. Although the reason for this is unknown, it is postulated that perhaps the initial suppression of autophagy in the F/F^{Cre} animals caused a need for increased muscle remodeling later in the recovery process compared to the F/F mice. Although not shown to be statistically significant by 2-way ANOVA, potential increases in the activity of calpain and cathepsin enzymes (which have both been shown to be involved with muscle remodeling)[100, 101] in the F/F^{Cre} animals compared to the F/F animals on day 14 support this theory.

Additional notable findings of the current study involved changes in fiber type distribution as a result of cardiotoxin exposure and potentially as a result of basal autophagy inhibition. Main effects of time showed a higher percentage of type IIA and IIB fibers on day 0, while an increased percentage of type IIA/X and IIX/B fibers was observed on day 14. The increase in hybrid fiber percentage on day 14 after cardiotoxin exposure likely demonstrates that fiber type transitions towards the basal fiber type composition were still occurring at this time since changes in myosin heavy chain composition occur along a continuum[102]. Cardiotoxin exposure also resulted in an increase in the total number of fibers in the muscle on day 14;

however, this was likely driven by the fact that some areas of the muscle cross-sections contained numerous fibers that were much smaller than normal (and likely still regenerating) at this time point. Interestingly, although not found to be statistically significant by 2-way ANOVA, a seemingly increased type IIA fiber percentage in conjunction with a seemingly decreased type IIB fiber percentage in the F/F^{Cre} animals on day 0 may suggest that autophagy inhibition under basal conditions causes a glycolytic-to-oxidative fiber type shift. Indeed, when autophagic function was restored in these mice on day 14, similar type IIA and IIB fiber distribution was observed between groups. Previous work by Moresi et al. reported a similar shift towards an increased proportion of oxidative fibers as a result of autophagy inhibition caused by HDAC1 and HDAC2 double knockout[103]. The proposed fiber type switch away from glycolytic type IIB fibers and towards oxidative type IIA fibers in the autophagy-deficient F/F^{Cre} mice in the current thesis may have been caused by the increased reliance on autophagy in glycolytic fibers as mentioned earlier.

Alterations in fiber type-specific and whole muscle cross-sectional area were also observed between the F/F and F/F^{Cre} animals. While similar fiber type-specific cross-sectional areas were observed between groups in all fiber types on day 0, type IIA, IIX, and IIX/B fiber CSA increased on day 14 in the F/F^{Cre} mice but not in the F/F mice. Despite a lack of statistical significance, it seems as though type IIA/X and IIB fiber CSA was also increased in the F/F^{Cre} animals on day 14. These increases in fiber-type specific CSA were accompanied by a statistical trend towards increased whole muscle cross-sectional area. While this study did not find any results to explain why muscle fiber hypertrophy occurred in the F/F^{Cre} group, one potential explanation involves insulin. Insulin is a peptide hormone that mediates the uptake of glucose into skeletal muscle, and also promotes protein synthesis and hypertrophy in skeletal muscle[104,

[105]. Prior research has suggested that autophagy inhibition may promote insulin resistance and elevated levels of circulating insulin[73, 106-108]. Consequently, it is possible that the initial autophagy inhibition in the F/F^{Cre} mice led to muscle insulin resistance and increased levels of circulating insulin. However, upon restoration of ATG7 expression and autophagic function, the muscles of the F/F^{Cre} mice may have regained their sensitivity to insulin. This improved insulin sensitivity along with temporarily increased levels of circulating insulin may have led to muscle fiber hypertrophy. Nevertheless, this theory is merely speculative as no measures of insulin sensitivity or circulating insulin were conducted in this study.

Limitations

Despite previous interesting findings in the inducible, skeletal muscle-specific Atg7 knockdown mice, it appears as though this model (at least when Cre recombination is driven by the HSA promoter) is not suitable for the study of extensive muscle damage. The restoration of ATG7 expression in the F/F^{Cre} mice upon muscle injury was clearly a major limitation of this study, and it prevented truly answering the question of whether autophagy serves a cytoprotective or cytotoxic role in skeletal muscle. Additionally, the lower level of ATG7 knockdown achieved in this study compared to other studies in the literature limited the ability to make strong conclusions regarding the effects of autophagy on the cellular environment and on apoptotic signaling under basal conditions. Moreover, we did not visualize possible abnormalities in organelle (e.g. mitochondria, sarcoplasmic reticulum) structure or sarcomere organization, or directly visualize autophagic flux (i.e. the formation and degradation of autophagosomes) under basal conditions or post-injury. The systemic administration of tamoxifen (i.e. via intraperitoneal injection) could also be viewed as a limitation since it may act on other tissues and/or have other effects independent of inducing Atg7 knockdown. However, it is very unlikely that the amount of tamoxifen administered in this study (2mg/day x 5 days = 10mg) had any toxic effects as the LD_{50} for tamoxifen via intraperitoneal delivery has been shown to be ~200mg/kg in mice[109]. Furthermore, although there is a small chance that systemic administration of tamoxifen affected the muscle's response to cardiotoxin-induced damage, it is unlikely that differences between genotypes existed since both groups were treated with tamoxifen. It is also unlikely that tamoxifen altered basal autophagic signaling on its own as pilot studies revealed similar levels of ATG7, p62, LCB-I, and LC3B-II between tamoxifen-treated and saline-treated F/F animals (data not shown). Another limitation of this study was that, as

discussed above, the expression levels of various proteins such as ATG7 that were detected by immunoblotting likely represented expression not only in the muscle cells but also in infiltrating immune cells and other cell types such as blood cells. The presence of these other cells within the muscle may have artificially increased various protein contents that were assumed to signify muscle protein expression. The use of meloxicam as an analgesic agent after cardiotoxin treatment also represents a limitation since meloxicam is a non-steroidal anti-inflammatory drug (NSAID). This may have blunted the inflammatory response to muscle damage and altered the autophagic and apoptotic signaling normally associated with muscle damage and regeneration. Notably, injections of meloxicam were only given immediately after and 24 hours post-cardiotoxin injection (i.e. meloxicam was not administered throughout the study period). Additionally, it is unlikely that differences between genotypes existed since meloxicam was administered to both groups. Finally, the temporal evaluation of autophagic and apoptotic signaling was somewhat limited in this study as only 4 time points were analyzed. Conducting analysis on a greater number of days would further elucidate the relationship between these two signaling pathways after acute muscle injury.

Future directions

Continuing tamoxifen treatment throughout the study protocol (i.e. after cardiotoxin injection until day 14) may prevent the restoration of ATG7 expression in the F/F^{Cre} mice, although the exact time required for tamoxifen-induced gene recombination to occur is not known. Therefore, short-term restoration of ATG7 may still occur despite continuous tamoxifen administration because of satellite cell fusion, as it may take some time before tamoxifen-induced gene recombination occurs in these new myonuclei. After gene recombination, it would also take time to degrade the ATG7 protein in the muscle that was generated by the satellite cells/new myonuclei. In future studies, it would also be helpful if the level of Atg7 knockdown was greater than that achieved in the current study. Since only a reduction of ~61% in ATG7 content was observed in the gastrocnemius on day 0, it is very possible that gene recombination did not take place in all of the myonuclei of the F/F^{Cre} animals. Consequently, unaffected $Atg7^{+/+}$ myonuclei may have still been capable of upregulating ATG7 expression in response to cardiotoxin damage. Increased doses of tamoxifen may help to increase the level of Atg7 knockdown by affecting a larger proportion of the muscle nuclei. Additionally, a longer "gene knockdown period" prior to cardiotoxin injection may cause greater reductions in ATG7 content as ATG7 expression was shown to be decreased by ~87% in undamaged quadriceps which were analyzed on day 14 which technically represented a "gene knockdown period" of 4 weeks. However, the variation in ATG7 knockdown between gastrocnemius and quadriceps could simply represent muscle-specific differences, and allowing 4 weeks to pass prior to cardiotoxin treatment would decrease the acute nature of the autophagy inhibition and increase the chance that the muscle would make compensatory changes as an adaptation to the autophagy deficiency.

Another possible approach to study the interplay between autophagy and muscle damage in inducible Atg7 knockdown mice in the future could be to find a stress that is less intense than cardiotoxin. If the stress was less extreme, it is possible that less satellite cell recruitment would occur and in turn the inhibition of autophagy would have a greater chance to persist. Eccentric exercise is thought to cause muscle damage, but the damage is believed to be limited to the excitation-contraction system and the force-bearing structures of the muscle (e.g. z-line, myosin crossbridges, myotendinous junction)[110]. In fact, Warren and colleagues concluded that dysfunction in the excitation-contraction coupling process (i.e. the events that occur between acetylcholine release at the neuromuscular junction and Ca2+ release from the sarcoplasmic reticulum) was responsible for up to 75% of the force decrease seen after eccentric exercise, with the remaining force deficit being caused by alterations and/or physical disruption to the force-bearing structures[111]. One reason for this conclusion was the fact that these authors were able to eliminate a 43% eccentric exercise-induced decrease in maximal isometric tetanic force by incubating the muscle with caffeine (which increases Ca2+ release from the sarcoplasmic reticulum)[111]. Additionally, Lo Verso and colleagues found no signs of major morphological damage (i.e. inflammation, necrosis, plasma membrane disruption) in tamoxifen-inducible, skeletal muscle-specific Atg7 KO mice or control mice subjected to eccentric exercise[73]. In turn, eccentric exercise could potentially be considered less traumatic to the muscle than cardiotoxin exposure. Unfortunately, despite a potentially lower level of damage, an increase in satellite cell activity has still been observed in response to eccentric exercise[112-114]. Another possible method to induce muscle damage is to expose mice to the chemotherapeutic drug doxorubicin, as a small amount of literature has shown that intraperitoneal injection of doxorubicin is myotoxic in rats[95, 115]. In contrast, pilot studies for the current Master's thesis found that doxorubicin injection did

not lead to any visible signs of morphological damage, nor did it lead to increased activation of apoptotic enzymes (Appendix Figure A3, A4, A5, and A6). Consequently, the effectiveness of inducing muscle damage by eccentric exercise or doxorubicin administration in absence of a significant satellite cell response is uncertain.

Alternatively, rather than using inducible Atg7 knockdown mice, future studies may consider using constitutive Atg7 knockdown animals to study the relationship between autophagy inhibition, apoptotic signaling, and muscle damage. Judging from the literature discussed earlier, it is likely that greater Atg7 knockdown and autophagy inhibition occurs in the constitutive Atg7 knockdown animals, and fewer myonuclei remain $Atg7^{+/+}$. Furthermore, since the localization of Cre recombinase is not controlled by mutated estrogen receptors in this model, Cre is able to translocate freely to the nucleus and cause Atg7 deletion at all times under basal conditions, and could also translocate and cause gene recombination in new myonuclei after cardiotoxin exposure. However, as previously discussed, there are limitations with this model as well since the constitutive Atg7 knockdown animals could develop adaptations to the gene knockdown during development to compensate for the lack of autophagy. One example of such an adaptation is that constitutive Atg7 knockout mice studied by Masiero and colleagues displayed a decreased amount of centrally nucleated fibers in comparison to inducible, skeletal muscle-specific Atg7 knockout mice[72]. Moreover, it is speculated that some restoration of ATG7 protein expression would be an issue in the constitutive Atg7 knockdown animals as well, at least for a period of time. This is because upon muscle damage, satellite cells would still be recruited and, like in the inducible Atg7 knockdown model, these satellite cell nuclei would still possess the Atg7 gene at first. Upon fusing to the damaged muscle fibers, these nuclei would produce the Cre recombinase enzyme necessary for gene knockdown, but would also produce

some ATG7 protein prior to Cre-mediated recombination of the Atg7 gene. This newly generated ATG7 protein could then support autophagic flux for a period of time before its natural degradation occurred. It is possible that the expression of ATG7 during this time would mask any conclusions regarding the true effects of autophagy inhibition during the initiation of muscle damage.

Because of the limitations in both inducible and constitutive Atg7 knockdown animals, it seems as though the best way to study the relationship between autophagy inhibition, apoptotic signaling, and muscle damage would be to induce Atg7 knockdown in both the myonuclei and the satellite cells prior to injury. This could potentially be accomplished by breeding the inducible mice used in this study with similar inducible mice where Cre transcription is driven by a satellite cell-specific marker such as Pax7. However, the inhibition of autophagy in satellite cells may also present a problem. A study by Tang & Rando found that inhibiting autophagy in satellite cells using chloroquine (a lysosomal inhibitor) or 3-methyladenine (a PI3K inhibitor) suppressed satellite cell activation[116]. Furthermore, they found that SIRT1 (a nutrient sensor) regulated autophagy during satellite cell activation, and that the inhibition of autophagy due to sirt1 knockout in satellite cells suppressed their activation[116]. In other words, autophagy inhibition in satellite cells may prevent their recruitment to the muscle fibers, causing a regenerative issue upstream of the effects of autophagy inhibition in the muscle itself. Further research into the inhibition of autophagy in both satellite cells and myonuclei should be conducted to see if this causes a lasting suppression of autophagy upon muscle injury without interfering with satellite cell recruitment.

Conclusions

In conclusion, although this thesis was not able to truly examine the changes in apoptotic signaling and muscle recovery in response to autophagy inhibition, it was able to further elucidate the relationship between autophagy and apoptosis after acute muscle injury. In fact, the results of this study seem to indicate a cytoprotective role for autophagy in response to muscle damage by blunting increases in cell stress and suppressing apoptotic signaling. This study also demonstrated that basal autophagy inhibition may alter fiber type distribution, and that a restoration of autophagy in previously autophagy-deficient muscle can potentially restore muscle fiber type composition and enhance muscle mass. Finally, this thesis discovered valuable methodological information for future studies as it showed that tamoxifen-inducible, skeletal muscle-specific knockdown models where Cre recombinase expression is driven by the HSA promoter should not be used in conditions of extensive muscle damage that causes satellite cell recruitment. Future research examining the effects of inducible gene manipulation during conditions of muscle damage should consider inducing a knockout in both myonuclei and satellite cells.

References

1. Raffaello A, Milan G, Masiero E, et al. JunB transcription factor maintains skeletal muscle mass and promotes hypertrophy. J Cell Biol 2010; 191: 101-113.

2. Charge SB and Rudnicki MA. Cellular and molecular regulation of muscle regeneration. Physiol Rev 2004; 84: 209-238.

3. Brooks SV and Faulkner JA. Contraction-induced injury: recovery of skeletal muscles in young and old mice. Am J Physiol 1990; 258: C436-42.

4. Wagers AJ and Conboy IM. Cellular and molecular signatures of muscle regeneration: current concepts and controversies in adult myogenesis. Cell 2005; 122: 659-667.

5. Brack AS and Rando TA. Tissue-specific stem cells: lessons from the skeletal muscle satellite cell. Cell Stem Cell 2012; 10: 504-514.

6. Ciciliot S and Schiaffino S. Regeneration of mammalian skeletal muscle. Basic mechanisms and clinical implications. Curr Pharm Des 2010; 16: 906-914.

7. Schiaffino S, Dyar KA, Ciciliot S, et al. Mechanisms regulating skeletal muscle growth and atrophy. FEBS J 2013; 280: 4294-4314.

8. Meijer AJ and Codogno P. Autophagy: regulation and role in disease. Crit Rev Clin Lab Sci 2009; 46: 210-240.

9. Lin PH, Duann P, Komazaki S, et al. Lysosomal two-pore channel subtype 2 (TPC2) regulates skeletal muscle autophagic signaling. J Biol Chem 2015; 290: 3377-3389.

10. Mammucari C, Milan G, Romanello V, et al. FoxO3 controls autophagy in skeletal muscle in vivo. Cell Metab 2007; 6: 458-471.

11. Adams J. The proteasome: structure, function, and role in the cell. Cancer Treat Rev 2003; 29 Suppl 1: 3-9.

12. Sandri M. Protein breakdown in muscle wasting: role of autophagy-lysosome and ubiquitin-proteasome. Int J Biochem Cell Biol 2013; 45: 2121-2129.

13. Bodine SC and Baehr LM. Skeletal muscle atrophy and the E3 ubiquitin ligases MuRF1 and MAFbx/atrogin-1. Am J Physiol Endocrinol Metab 2014; 307: E469-84.

14. Levine B, Mizushima N and Virgin HW. Autophagy in immunity and inflammation. Nature 2011; 469: 323-335.

15. Kroemer G, Marino G and Levine B. Autophagy and the integrated stress response. Mol Cell 2010; 40: 280-293.

16. Tanida I, Ueno T and Kominami E. LC3 conjugation system in mammalian autophagy. Int J Biochem Cell Biol 2004; 36: 2503-2518.

17. Masiero E, Agatea L, Mammucari C, et al. Autophagy is required to maintain muscle mass. Cell Metab 2009; 10: 507-515.

18. Komatsu M, Waguri S, Ueno T, et al. Impairment of starvation-induced and constitutive autophagy in Atg7-deficient mice. J Cell Biol 2005; 169: 425-434.

19. Kim KH, Jeong YT, Oh H, et al. Autophagy deficiency leads to protection from obesity and insulin resistance by inducing Fgf21 as a mitokine. Nat Med 2013; 19: 83-92.

20. Nakai A, Yamaguchi O, Takeda T, et al. The role of autophagy in cardiomyocytes in the basal state and in response to hemodynamic stress. Nat Med 2007; 13: 619-624.

21. Pattison JS, Osinska H and Robbins J. Atg7 induces basal autophagy and rescues autophagic deficiency in CryABR120G cardiomyocytes. Circ Res 2011; 109: 151-160.

22. Mizushima N, Levine B, Cuervo AM, et al. Autophagy fights disease through cellular self-digestion. Nature 2008; 451: 1069-1075.

23. Lum JJ, Bauer DE, Kong M, et al. Growth factor regulation of autophagy and cell survival in the absence of apoptosis. Cell 2005; 120: 237-248.

24. Singh R and Cuervo AM. Autophagy in the cellular energetic balance. Cell Metab 2011; 13: 495-504.

25. Mizushima N. Autophagy: process and function. Genes Dev 2007; 21: 2861-2873.

26. Murrow L and Debnath J. Autophagy as a stress-response and quality-control mechanism: implications for cell injury and human disease. Annu Rev Pathol 2013; 8: 105-137.

27. Kaushik S, Singh R and Cuervo AM. Autophagic pathways and metabolic stress. Diabetes Obes Metab 2010; 12 Suppl 2: 4-14.

28. Elmore S. Apoptosis: a review of programmed cell death. Toxicol Pathol 2007; 35: 495-516.

29. Dupont-Versteegden EE. Apoptosis in skeletal muscle and its relevance to atrophy. World J Gastroenterol 2006; 12: 7463-7466.

30. Nunez G, Benedict MA, Hu Y, et al. Caspases: the proteases of the apoptotic pathway. Oncogene 1998; 17: 3237-3245.

31. Chipuk JE, Bouchier-Hayes L and Green DR. Mitochondrial outer membrane permeabilization during apoptosis: the innocent bystander scenario. Cell Death Differ 2006; 13: 1396-1402.

32. Favaloro B, Allocati N, Graziano V, et al. Role of apoptosis in disease. Aging (Albany NY) 2012; 4: 330-349.

33. Gordy C and He YW. The crosstalk between autophagy and apoptosis: where does this lead?. Protein Cell 2012; 3: 17-27.

34. Dupont-Versteegden EE. Apoptosis in muscle atrophy: relevance to sarcopenia. Exp Gerontol 2005; 40: 473-481.

35. Kroemer G, Marino G and Levine B. Autophagy and the integrated stress response. Mol Cell 2010; 40: 280-293.

36. Wirawan E, Vande Walle L, Kersse K, et al. Caspase-mediated cleavage of Beclin-1 inactivates Beclin-1-induced autophagy and enhances apoptosis by promoting the release of proapoptotic factors from mitochondria. Cell Death Dis 2010; 1: e18.

37. Romanov J, Walczak M, Ibiricu I, et al. Mechanism and functions of membrane binding by the Atg5-Atg12/Atg16 complex during autophagosome formation. EMBO J 2012; 31: 4304-4317.

38. Pyo JO, Jang MH, Kwon YK, et al. Essential roles of Atg5 and FADD in autophagic cell death: dissection of autophagic cell death into vacuole formation and cell death. J Biol Chem 2005; 280: 20722-20729.

39. Yousefi S, Perozzo R, Schmid I, et al. Calpain-mediated cleavage of Atg5 switches autophagy to apoptosis. Nat Cell Biol 2006; 8: 1124-1132.

40. Betin VM, MacVicar TD, Parsons SF, et al. A cryptic mitochondrial targeting motif in Atg4D links caspase cleavage with mitochondrial import and oxidative stress. Autophagy 2012; 8: 664-676.

41. Hou W, Han J, Lu C, et al. Autophagic degradation of active caspase-8: a crosstalk mechanism between autophagy and apoptosis. Autophagy 2010; 6: 891-900.

42. Marzetti E, Calvani R, Bernabei R, et al. Apoptosis in skeletal myocytes: a potential target for interventions against sarcopenia and physical frailty - a mini-review. Gerontology 2012; 58: 99-106.

43. Bruusgaard JC, Johansen IB, Egner IM, et al. Myonuclei acquired by overload exercise precede hypertrophy and are not lost on detraining. Proc Natl Acad Sci U S A 2010; 107: 15111-15116.

44. Ciciliot S and Schiaffino S. Regeneration of mammalian skeletal muscle. Basic mechanisms and clinical implications. Curr Pharm Des 2010; 16: 906-914.

45. Plant PJ, Bain JR, Correa JE, et al. Absence of caspase-3 protects against denervation-induced skeletal muscle atrophy. J Appl Physiol (1985) 2009; 107: 224-234.

46. Du J, Wang X, Miereles C, et al. Activation of caspase-3 is an initial step triggering accelerated muscle proteolysis in catabolic conditions. J Clin Invest 2004; 113: 115-123.

47. Supinski GS and Callahan LA. Caspase activation contributes to endotoxin-induced diaphragm weakness. J Appl Physiol (1985) 2006; 100: 1770-1777.

48. Fernando P, Kelly JF, Balazsi K, et al. Caspase 3 activity is required for skeletal muscle differentiation. Proc Natl Acad Sci U S A 2002; 99: 11025-11030.

49. Jin X, Qu N, He Y, et al. Cell apoptosis in atrophic skeletal muscle induced by immoblization in rabbits--an experimental study using TUNEL. Sheng Wu Yi Xue Gong Cheng Xue Za Zhi 2004; 21: 628-30, 635.

50. Dirks A and Leeuwenburgh C. Apoptosis in skeletal muscle with aging. Am J Physiol Regul Integr Comp Physiol 2002; 282: R519-27.

51. Vescovo G, Volterrani M, Zennaro R, et al. Apoptosis in the skeletal muscle of patients with heart failure: investigation of clinical and biochemical changes. Heart 2000; 84: 431-437.

52. Stratos I, Graff J, Rotter R, et al. Open blunt crush injury of different severity determines nature and extent of local tissue regeneration and repair. J Orthop Res 2010; 28: 950-957.

53. Stratos I, Li Z, Rotter R, et al. Inhibition of caspase mediated apoptosis restores muscle function after crush injury in rat skeletal muscle. Apoptosis 2012; 17: 269-277.

54. Wu JJ, Quijano C, Chen E, et al. Mitochondrial dysfunction and oxidative stress mediate the physiological impairment induced by the disruption of autophagy. Aging (Albany NY) 2009; 1: 425-437.

55. Masiero E and Sandri M. Autophagy inhibition induces atrophy and myopathy in adult skeletal muscles. Autophagy 2010; 6: 307-309.

56. Raben N, Hill V, Shea L, et al. Suppression of autophagy in skeletal muscle uncovers the accumulation of ubiquitinated proteins and their potential role in muscle damage in Pompe disease. Hum Mol Genet 2008; 17: 3897-3908.

57. O'Leary MF, Vainshtein A, Carter HN, et al. Denervation-induced mitochondrial dysfunction and autophagy in skeletal muscle of apoptosis-deficient animals. Am J Physiol Cell Physiol 2012; 303: C447-54.

58. Smuder AJ, Kavazis AN, Min K, et al. Exercise protects against doxorubicin-induced markers of autophagy signaling in skeletal muscle. J Appl Physiol (1985) 2011; 111: 1190-1198.

59. McCarthy JJ, Srikuea R, Kirby TJ, et al. Inducible Cre transgenic mouse strain for skeletal muscle-specific gene targeting. Skelet Muscle 2012; 2: 8-5040-2-8.

60. Nagy A. Cre recombinase: the universal reagent for genome tailoring. Genesis 2000; 26: 99-109.

61. Danielian PS, White R, Hoare SA, et al. Identification of residues in the estrogen receptor that confer differential sensitivity to estrogen and hydroxytamoxifen. Mol Endocrinol 1993; 7: 232-240.

62. Littlewood TD, Hancock DC, Danielian PS, et al. A modified oestrogen receptor ligand-binding domain as an improved switch for the regulation of heterologous proteins. Nucleic Acids Res 1995; 23: 1686-1690.

63. Brennan KJ and Hardeman EC. Quantitative analysis of the human alpha-skeletal actin gene in transgenic mice. J Biol Chem 1993; 268: 719-725.

64. Kam MK, Lee KY, Tam PK, et al. Generation of NSE-MerCreMer transgenic mice with tamoxifen inducible Cre activity in neurons. PLoS One 2012; 7: e35799.

65. Guo C, Yang W and Lobe CG. A Cre recombinase transgene with mosaic, widespread tamoxifen-inducible action. Genesis 2002; 32: 8-18.

66. McCarthy JJ, Mula J, Miyazaki M, et al. Effective fiber hypertrophy in satellite cell-depleted skeletal muscle. Development 2011; 138: 3657-3666.

67. McMillan EM and Quadrilatero J. Differential apoptosis-related protein expression, mitochondrial properties, proteolytic enzyme activity, and DNA fragmentation between skeletal muscles. Am J Physiol Regul Integr Comp Physiol 2011; 300: R531-43.

68. Tchoupe JR, Moreau T, Gauthier F, et al. Photometric or fluorometric assay of cathepsin B, L and H and papain using substrates with an aminotrifluoromethylcoumarin leaving group. Biochim Biophys Acta 1991; 1076: 149-151.

69. Dietrich N, Thastrup J, Holmberg C, et al. JNK2 mediates TNF-induced cell death in mouse embryonic fibroblasts via regulation of both caspase and cathepsin protease pathways. Cell Death Differ 2004; 11: 301-313.

70. McMillan EM, Pare MF, Baechler BL, et al. Autophagic signaling and proteolytic enzyme activity in cardiac and skeletal muscle of spontaneously hypertensive rats following chronic aerobic exercise. PLoS One 2015; 10: e0119382.

71. Jaisser F. Inducible gene expression and gene modification in transgenic mice. J Am Soc Nephrol 2000; 11 Suppl 16: S95-S100.

72. Masiero E, Agatea L, Mammucari C, et al. Autophagy is required to maintain muscle mass. Cell Metab 2009; 10: 507-515.

73. Lo Verso F, Carnio S, Vainshtein A, et al. Autophagy is not required to sustain exercise and PRKAA1/AMPK activity but is important to prevent mitochondrial damage during physical activity. Autophagy 2014; 10: 1883-1894.

74. Carnio S, LoVerso F, Baraibar MA, et al. Autophagy impairment in muscle induces neuromuscular junction degeneration and precocious aging. Cell Rep 2014; 8: 1509-1521.

75. Mizushima N, Yamamoto A, Matsui M, et al. In vivo analysis of autophagy in response to nutrient starvation using transgenic mice expressing a fluorescent autophagosome marker. Mol Biol Cell 2004; 15: 1101-1111.

76. Ogata T, Oishi Y, Higuchi M, et al. Fasting-related autophagic response in slow- and fast-twitch skeletal muscle. Biochem Biophys Res Commun 2010; 394: 136-140.

77. Kim KH, Jeong YT, Oh H, et al. Autophagy deficiency leads to protection from obesity and insulin resistance by inducing Fgf21 as a mitokine. Nat Med 2013; 19: 83-92.

78. Wu JJ, Quijano C, Chen E, et al. Mitochondrial dysfunction and oxidative stress mediate the physiological impairment induced by the disruption of autophagy. Aging (Albany NY) 2009; 1: 425-437.

79. Muscat GE and Kedes L. Multiple 5'-flanking regions of the human alpha-skeletal actin gene synergistically modulate muscle-specific expression. Mol Cell Biol 1987; 7: 4089-4099.

80. Yoshida N, Yoshida S, Koishi K, et al. Cell heterogeneity upon myogenic differentiation: down-regulation of MyoD and Myf-5 generates 'reserve cells'. J Cell Sci 1998; 111 (Pt 6): 769-779.

81. Morgan JE and Partridge TA. Muscle satellite cells. Int J Biochem Cell Biol 2003; 35: 1151-1156.

82. Ciciliot S and Schiaffino S. Regeneration of mammalian skeletal muscle. Basic mechanisms and clinical implications. Curr Pharm Des 2010; 16: 906-914.

83. Nagata Y, Partridge TA, Matsuda R, et al. Entry of muscle satellite cells into the cell cycle requires sphingolipid signaling. J Cell Biol 2006; 174: 245-253.

84. Tatsumi R, Liu X, Pulido A, et al. Satellite cell activation in stretched skeletal muscle and the role of nitric oxide and hepatocyte growth factor. Am J Physiol Cell Physiol 2006; 290: C1487-94.

85. Miller KJ, Thaloor D, Matteson S, et al. Hepatocyte growth factor affects satellite cell activation and differentiation in regenerating skeletal muscle. Am J Physiol Cell Physiol 2000; 278: C174-81.

86. Brack AS, Conboy IM, Conboy MJ, et al. A temporal switch from notch to Wnt signaling in muscle stem cells is necessary for normal adult myogenesis. Cell Stem Cell 2008; 2: 50-59.

87. Sesodia S, Choksi RM and Nemeth PM. Nerve-dependent recovery of metabolic pathways in regenerating soleus muscles. J Muscle Res Cell Motil 1994; 15: 573-581.

88. Turk V, Stoka V, Vasiljeva O, et al. Cysteine cathepsins: from structure, function and regulation to new frontiers. Biochim Biophys Acta 2012; 1824: 68-88.

89. Mammucari C, Milan G, Romanello V, et al. FoxO3 controls autophagy in skeletal muscle in vivo. Cell Metab 2007; 6: 458-471.

90. Korolchuk VI, Menzies FM and Rubinsztein DC. Mechanisms of cross-talk between the ubiquitin-proteasome and autophagy-lysosome systems. FEBS Lett 2010; 584: 1393-1398.

91. Charge SB and Rudnicki MA. Cellular and molecular regulation of muscle regeneration. Physiol Rev 2004; 84: 209-238.

92. Muller FL, Song W, Liu Y, et al. Absence of CuZn superoxide dismutase leads to elevated oxidative stress and acceleration of age-dependent skeletal muscle atrophy. Free Radic Biol Med 2006; 40: 1993-2004.

93. Wei MC, Lindsten T, Mootha VK, et al. tBID, a membrane-targeted death ligand, oligomerizes BAK to release cytochrome c. Genes Dev 2000; 14: 2060-2071.

94. O'Leary MF, Vainshtein A, Carter HN, et al. Denervation-induced mitochondrial dysfunction and autophagy in skeletal muscle of apoptosis-deficient animals. Am J Physiol Cell Physiol 2012; 303: C447-54.

95. Smuder AJ, Kavazis AN, Min K, et al. Exercise protects against doxorubicin-induced markers of autophagy signaling in skeletal muscle. J Appl Physiol (1985) 2011; 111: 1190-1198.

96. Bargiela A, Cerro-Herreros E, Fernandez-Costa JM, et al. Increased autophagy and apoptosis contribute to muscle atrophy in a myotonic dystrophy type 1 Drosophila model. Dis Model Mech 2015; 8: 679-690.

97. McMillan EM and Quadrilatero J. Autophagy is required and protects against apoptosis during myoblast differentiation. Biochem J 2014; 462: 267-277.

98. Bloemberg D and Quadrilatero J. Mitochondrial pro-apoptotic indices do not precede the transient caspase activation associated with myogenesis. Biochim Biophys Acta 2014; 1843: 2926-2936.

99. Kabeya Y, Mizushima N, Ueno T, et al. LC3, a mammalian homologue of yeast Apg8p, is localized in autophagosome membranes after processing. EMBO J 2000; 19: 5720-5728.

100. Huang J and Forsberg NE. Role of calpain in skeletal-muscle protein degradation. Proc Natl Acad Sci U S A 1998; 95: 12100-12105.

101. Maltz L and Oron U. Proteolytic enzyme activities during regeneration of the rat gastrocnemius muscle. J Neurol Sci 1990; 98: 149-154.

102. Zhang MY, Zhang WJ and Medler S. The continuum of hybrid IIX/IIB fibers in normal mouse muscles: MHC isoform proportions and spatial distribution within single fibers. Am J Physiol Regul Integr Comp Physiol 2010; 299: R1582-91.

103. Moresi V, Carrer M, Grueter CE, et al. Histone deacetylases 1 and 2 regulate autophagy flux and skeletal muscle homeostasis in mice. Proc Natl Acad Sci U S A 2012; 109: 1649-1654.

104. Abdul-Ghani MA and DeFronzo RA. Pathogenesis of insulin resistance in skeletal muscle. J Biomed Biotechnol 2010; 2010: 476279.

105. Bolster DR, Jefferson LS and Kimball SR. Regulation of protein synthesis associated with skeletal muscle hypertrophy by insulin-, amino acid- and exercise-induced signalling. Proc Nutr Soc 2004; 63: 351-356.

106. Liu Y, Palanivel R, Rai E, et al. Adiponectin stimulates autophagy and reduces oxidative stress to enhance insulin sensitivity during high-fat diet feeding in mice. Diabetes 2015; 64: 36-48.

107. Martinez-Lopez N, Athonvarangkul D, Sahu S, et al. Autophagy in Myf5+ progenitors regulates energy and glucose homeostasis through control of brown fat and skeletal muscle development. EMBO Rep 2013; 14: 795-803.

108. Yang L, Li P, Fu S, et al. Defective hepatic autophagy in obesity promotes ER stress and causes insulin resistance. Cell Metab 2010; 11: 467-478.

109. Furr BJ and Jordan VC. The pharmacology and clinical uses of tamoxifen. Pharmacol Ther 1984; 25: 127-205.

110. Proske U and Morgan DL. Muscle damage from eccentric exercise: mechanism, mechanical signs, adaptation and clinical applications. J Physiol 2001; 537: 333-345.

111. Warren GL, Ingalls CP, Lowe DA, et al. Excitation-contraction uncoupling: major role in contraction-induced muscle injury. Exerc Sport Sci Rev 2001; 29: 82-87.

112. Darr KC and Schultz E. Exercise-induced satellite cell activation in growing and mature skeletal muscle. J Appl Physiol (1985) 1987; 63: 1816-1821.

113. Hyldahl RD, Olson T, Welling T, et al. Satellite cell activity is differentially affected by contraction mode in human muscle following a work-matched bout of exercise. Front Physiol 2014; 5: 485.

114. Valero MC, Huntsman HD, Liu J, et al. Eccentric exercise facilitates mesenchymal stem cell appearance in skeletal muscle. PLoS One 2012; 7: e29760.

115. Smuder AJ, Kavazis AN, Min K, et al. Exercise protects against doxorubicin-induced oxidative stress and proteolysis in skeletal muscle. J Appl Physiol (1985) 2011; 110: 935-942.

116. Tang AH and Rando TA. Induction of autophagy supports the bioenergetic demands of quiescent muscle stem cell activation. EMBO J 2014; 33: 2782-2797.

Appendix

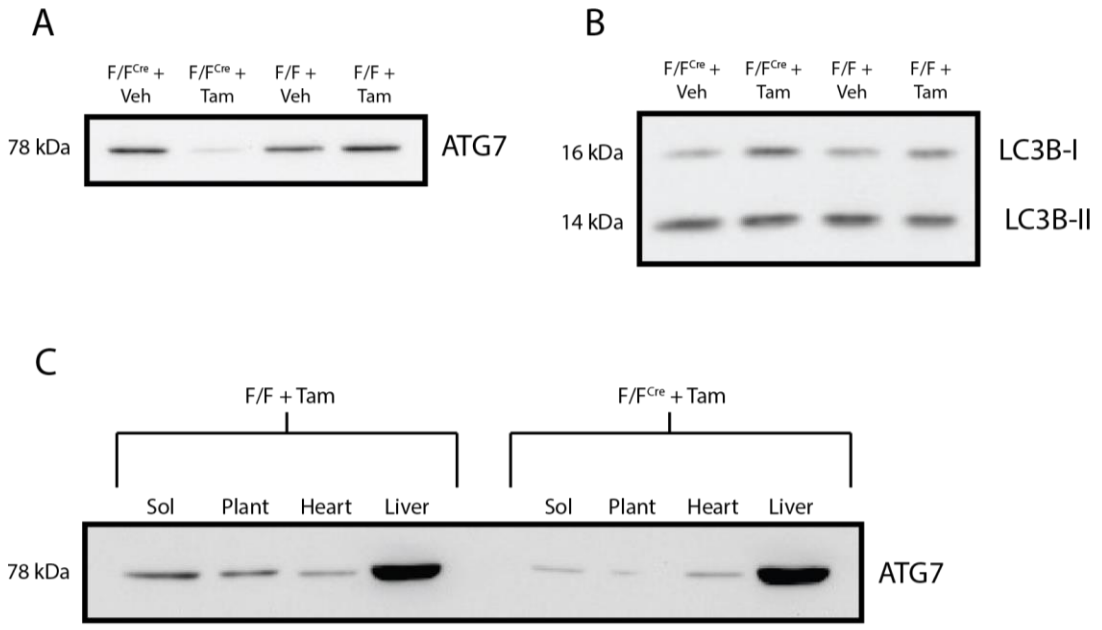

Figure A1: Validation of the tamoxifen-inducible, skeletal muscle-specific Atg7 knockdown model. Representative immunoblot two weeks post-treatment showing soleus Atg7 protein content from Atg7 F/F and Atg7 F/F^{Cre} animals treated with vehicle or tamoxifen (A). Representative immunoblot showing LC3B protein levels from Atg7 F/F and Atg7 F/F^{Cre} animals treated with vehicle or tamoxifen (B). Although there is no visible decrease in LC3B-II, the accumulation of LC3B-I in the Atg7 F/F^{Cre} mice suggests an inhibition of the conversion of LC3B-I to LC3B-II which will inhibit autophagy. Representative immunoblot showing the skeletal muscle-specific nature of Atg7 protein knockdown in the tamoxifen-treated F/F^{Cre} mice (C).

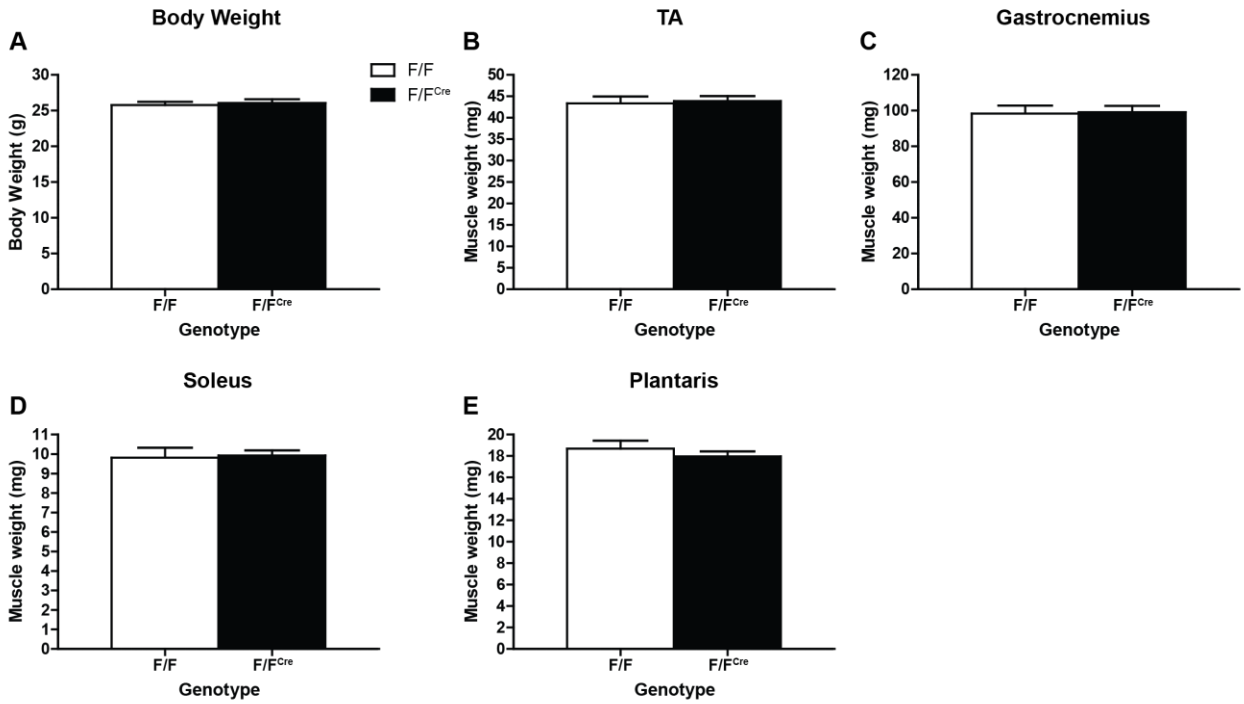

Figure A2: Body weight and absolute muscle weights on day 14. Quantification of body weight (A), absolute TA (B), gastrocnemius (C), soleus (D), and plantaris (E) muscle weights (n=8 per group). No significant differences were observed by Student's t-tests.

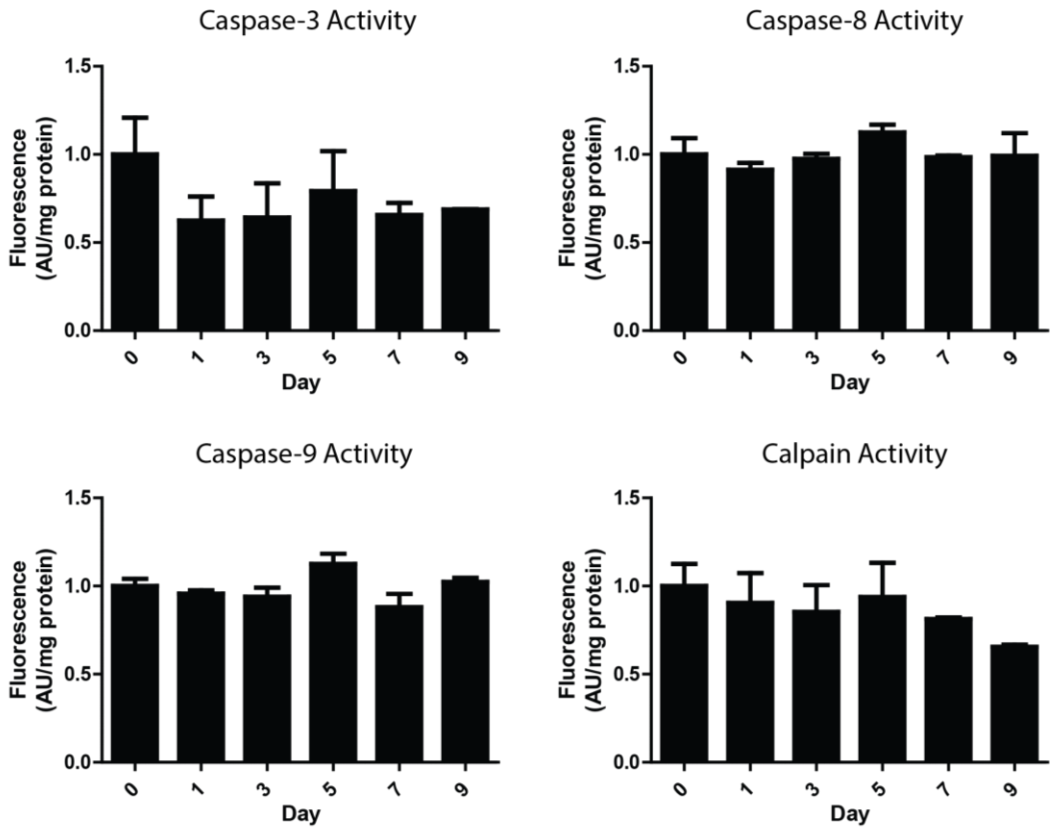

Figure A3: Apoptotic enzyme activity in C57 mice in response to doxorubicin exposure (n=3 per day). Days listed represent the number of days after doxorubicin treatment, with day 0 being a basal measurement prior to injection. No significant increases in apoptotic enzyme activities were observed in gastrocnemius on any day relative to day 0.

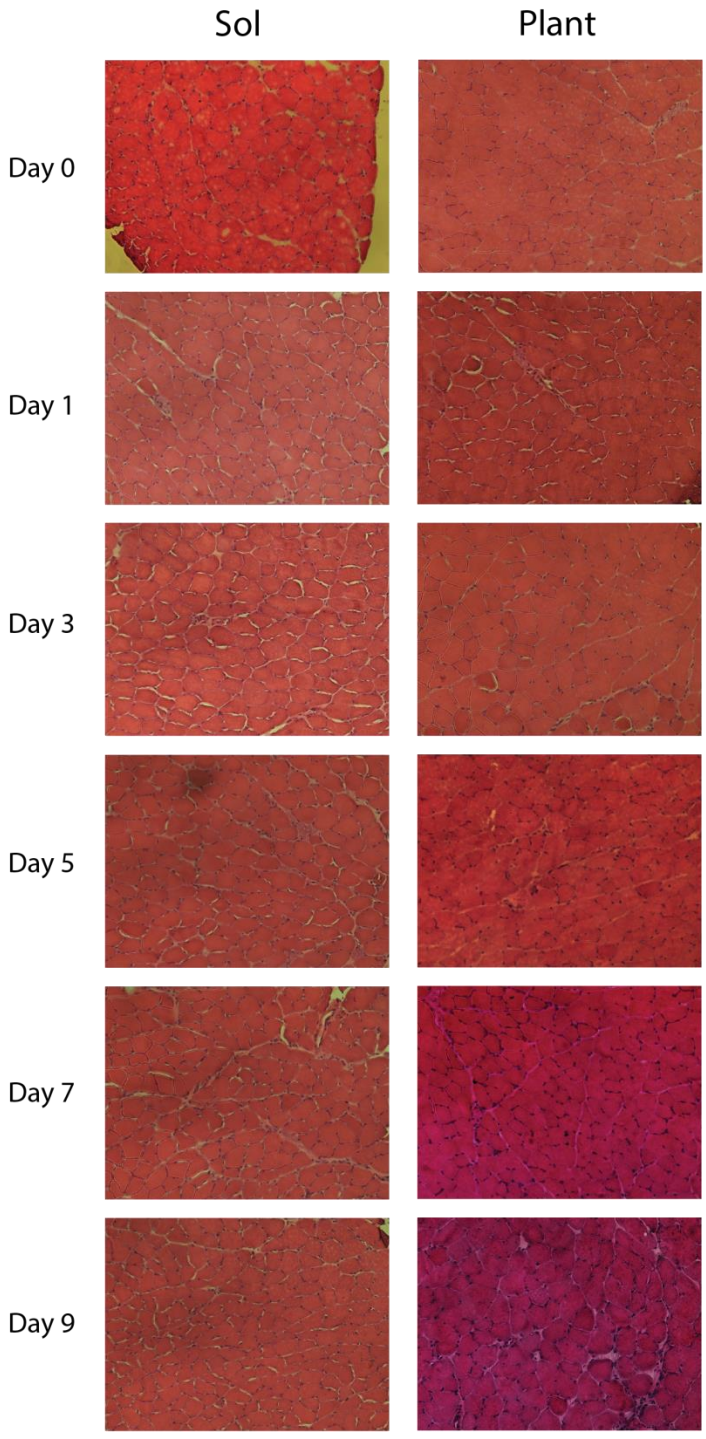

Figure A4: Morphological analysis of muscle damage in response to doxorubicin treatment. Days listed represent the number of days after doxorubicin treatment, with day 0 being a basal measurement prior to injection. No major differences in morphology were observed at any time point compared to day 0. Sol: soleus. Plant: plantaris.

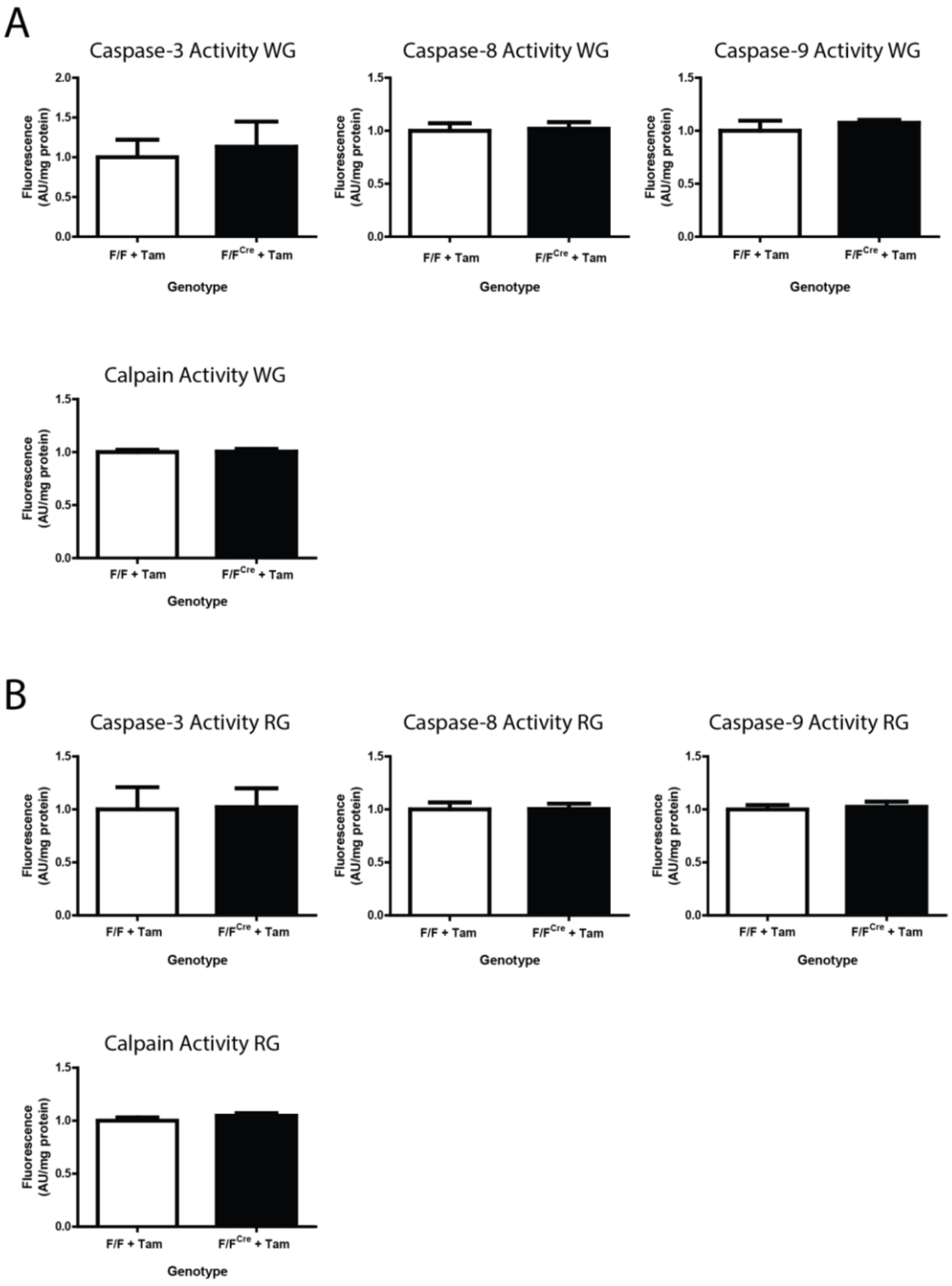

Figure A5: Apoptotic enzyme activity of F/F and F/F^{Cre} mice treated with both tamoxifen and doxorubicin (n=4 per group). All mice were sacrificed 4 days after doxorubicin injection in an attempt to allow enough time for doxorubicin to cause muscle damage. No differences in apoptotic enzyme activities were observed between the F/F and F/F^{Cre} (autophagy deficient) mice. RG: red gastrocnemius. WG: white gastrocnemius.

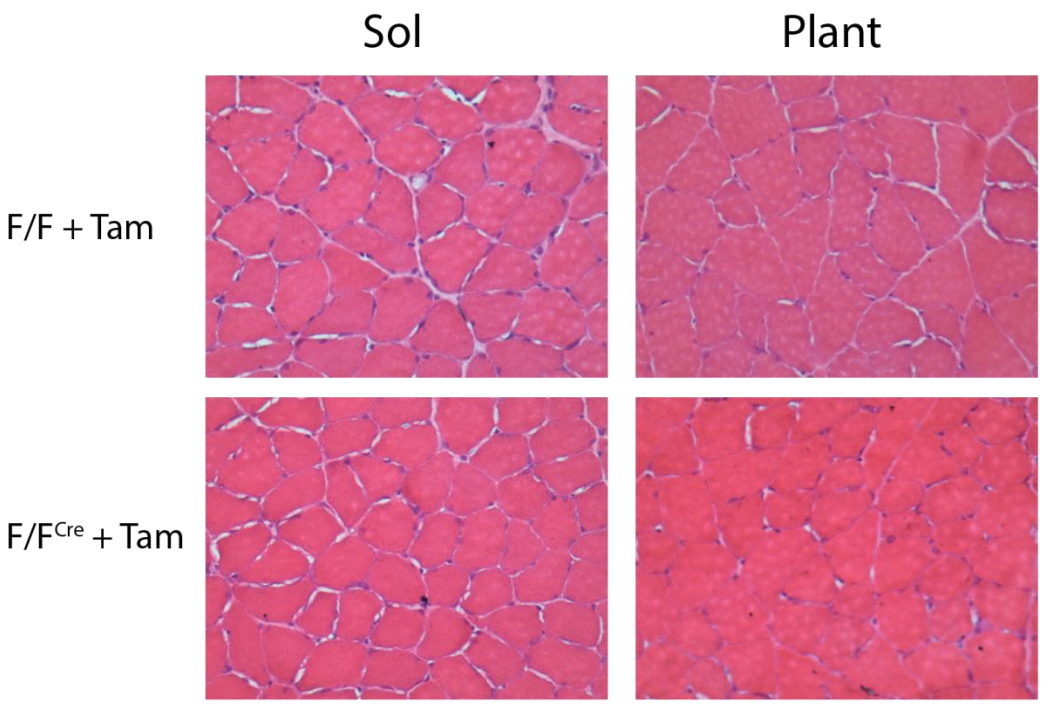

Figure A6: Morphological analysis of muscle damage in F/F and F/F^{Cre} mice treated with both tamoxifen and doxorubicin. All mice were sacrificed 4 days after doxorubicin injection in an attempt to allow enough time for doxorubicin to cause muscle damage. No major differences in morphology were observed between the F/F and F/F^{Cre} (autophagy deficient) mice. Sol: soleus. Plant: plantaris.